DISSERTATIONS IN
FORESTRY AND
NATURAL SCIENCES

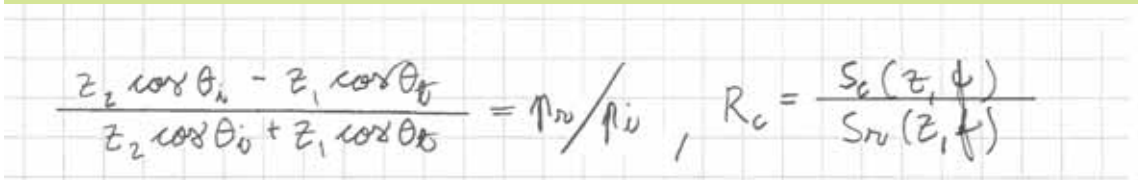

JUKKA LIUKKONEN

Ultrasound Arthroscopy of Articular Cartilage and Subchondral Bone

Clinical and Numerical Studies

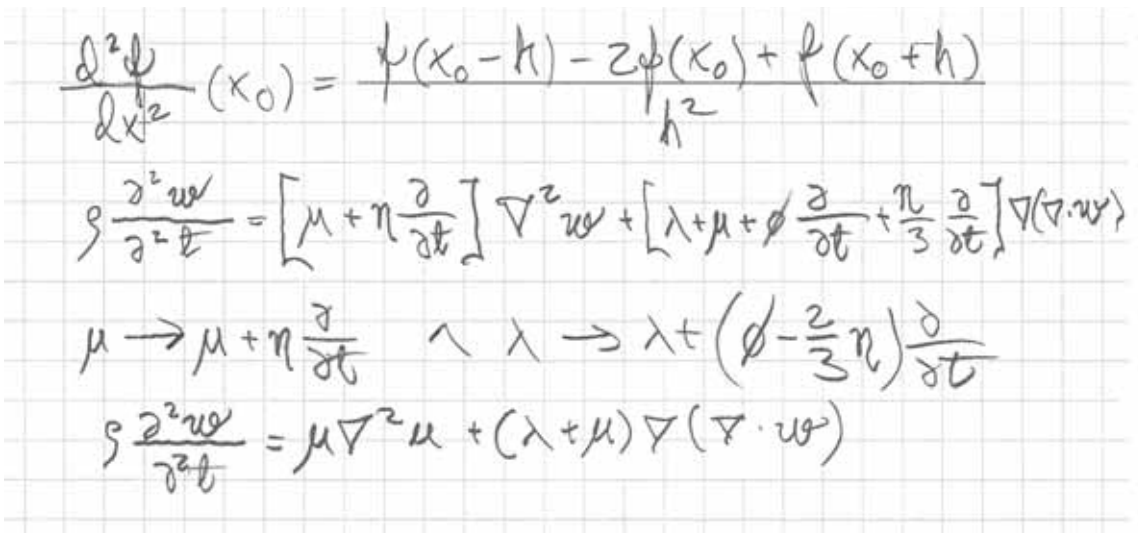

PUBLICATIONS OF THE UNIVERSITY OF EASTERN FINLAND
Dissertations in Forestry and Natural Sciences

UNIVERSITY OF
EASTERN FINLAND

JUKKA LIUKKONEN

Ultrasound Arthroscopy of Articular Cartilage and Subchondral Bone

Clinical and Numerical Studies

Publications of the University of Eastern Finland
Dissertations in Forestry and Natural Sciences
No 174

Academic Dissertation
To be presented by permission of the Faculty of Science and Forestry for public examination in the Auditorium MD100 in Mediteknia Building at the University of Eastern Finland, Kuopio, on May, 9, 2015,
at 12 o'clock noon.

Department of Applied Physics

Kopio Niini Oy
Kuopio, 2015
Editors: Prof. Pertti Pasanen, Prof. Pekka Kilpeläinen,
Prof. Kai Peiponen, Prof. Matti Vornanen

Distribution:
University of Eastern Finland Library / Sales of publications
P.O. Box 107, FI-80101 Joensuu, Finland tel. +358-50-3058396
julkaisumyynti@uef.fi
http://www.uef.fi/kirjasto

ISBN: 978-952-61-1756-0 (printed)
ISBN: 978-952-61-1757-7 (PDF)
ISSNL: 1798-5668
ISSN: 1798-5668
ISSN: 1798-5676 (PDF)

Author's address:
University of Eastern Finland
Department of Applied Physics
P.O.Box 1627
70211 KUOPIO
FINLAND
email: jukka.liukkonen@uef.fi

Supervisors:
Professor Juha Töyräs, Ph.D.
University of Eastern Finland
Department of Applied Physics
mail: juha.toyras@uef.fi

Professor Jukka Jurvelin, Ph.D.
University of Eastern Finland
Department of Applied Physics
email: jukka.jurvelin@uef.fi

Reviewers:
Associate Professor Jonathan J. Kaufman, Ph.D.
The Mount Sinai School of Medicine
Department of Orthopedics
New York, NY, USA
email: jjkaufman@cyberlogic.org

Professor Sharmila Majumdar, Ph.D.
University of California, San Francisco
School of Medicine, Department of Radiology
and Biomedical Imaging
San Francisco, CA, USA
email: sharmila.majumdar@ucsf.edu

Opponent:
Professor Stuart F. Foster, Ph.D.
University of Toronto
Department of Medical Biophysics
Toronto, Canada
email: stuart.foster@sri.utoronto.ca

ABSTRACT

Arthroscopy is one of the most common orthopedic operations and millions of arthroscopies are annually performed worldwide. Arthroscopic diagnosis should be immediate, sensitive and reproducible to optimize surgical treatments and to indicate therapies in order to combat trauma-initiated osteoarthritis (OA). During traditional arthroscopy, the severity and extent of cartilage defects are evaluated by means of visual inspection and palpation. In the diagnosis, these findings are collated together other with preoperative information *e.g.* those obtained with external palpation, radiographic imaging or magnetic resonance imaging. However, the conventional arthroscopic evaluation of cartilage is subjective and poorly reproducible. Thus, more quantitative arthroscopic methods to diagnose cartilage lesions are warranted.

Quantitative ultrasound imaging, conducted during arthroscopy (ultrasound arthoscopy), enables the detection of cartilage injuries as well as the early signs of spontaneous OA. Nevertheless, the optimization of this technique requires that the effect of cartilage structure and composition on ultrasound propagation must be understood. In addition, the clinical feasibility of quantitative ultrasound for simultaneous evaluation of cartilage and subchondral bone has not been examined in any detail.

In this thesis, the feasibility of using the ultrasound arthroscopy technique in the diagnostics of joint disorders was investigated *in vitro* and *in vivo*, and ultrasound interactions in cartilage tissue were modeled using the finite difference time domain (FDTD) method.

In studies I and II, the simultaneous ultrasound assessment of articular cartilage and subchondral bone was evaluated *in vitro* and *in vivo*. In study III, numerical models for ultrasound reflection from articular surfaces with varying surface roughnesses, material properties and angles of ultrasound incidence were constructed. Study IV introduced a sample specific transversely isotropic numerical model of ultrasound propagation in articular cartilage containing chondrocytes, proteoglycans (PG), collagen and water.

In study I, significant correlations were detected between ultrasound parameters and radiographic subchondral bone properties (volume fraction, mineral density, surface/volume ratio and trabecular thickness). Furthermore, in study II, the inclusion of ultrasound during arthroscopy was shown to significantly affect the evaluation of cartilage integrity by increasing ICRS grades compared to those based on conventional visual arthroscopy. In study III, the significant correlations were revealed *in vitro* between the ultrasound reflection at cartilage surface and the state of the cartilage. The results of FDTD models for ultrasound reflection and propagation in cartilage agreed with both current and previously published experimental studies. The present models provided sample specific implementation of surface roughness and cartilage composition. In study IV, a significant correlation was revealed between the experimental and simulated SOS. The effects of depletion of solid components agreed with the results in previous literature.

To conclude, ultrasound arthroscopy was found to provide valuable information on cartilage. The ultrasound probe used in the present studies was originally designed for intravascular use and is not optimal for ultrasound arthroscopy. The numerical models introduced in this thesis may provide significant help in the interpretation of the results of ultrasound assessment of cartilage and subchondral bone. However, further development will be needed before there can be routine clinical use of these techniques.

National Library of Medicine Classification: QT 34.5, QT 36, WE 300, WE 304, WN 208

Medical Subject Headings: Cartilage, Articular; Elastic Tissue; Bone and Bones; Joint Diseases/diagnosis; Osteoarthritis; Arthroscopy; Biomechanical Phenomena; Elasticity; Ultrasonics; Ultrasonography; Numerical Analysis, Computer-Assisted; Computer Simulation

Yleinen suomalainen asiasanasto: nivelrusto; nivelrikko; luu; biomekaniikka; kimmoisuus; joustavuus; ultraääni; ultraäänitutkimus; kuvantaminen; numeerinen analyysi

Acknowledgements

First, I would like to express my appreciation to all the patients who have participated in this study.

This study was carried out in the Department of Applied Physics, University of Eastern Finland and Kuopio University Hospital. I wish to offer my sincere thanks to all of you who have participated or otherwise contributed to my research work.

I have had the privilege to have a series of math and science teachers on my journey through the school system. I want to express how grateful I am to my teachers Kari Willman, Matti Mustonen and Jouko Tanninen. With them I became fascinated with the wonders of science. Especially, I wish to thank Rauno Perälä who has been there for me since the high school.

Professor Juha Töyräs, I express my deepest gratitude for the continuous guidance. I admire your enthusiasm, hard work, impressive knowledge and particular sense of humour.

Professor Jukka Jurvelin, my genuine thanks for critical support and being an approachable and warm-hearted mentor.

I owe my deepest gratitude to the official reviewers of this thesis Associate Professor Jonathan J. Kaufman and Professor Sharmila Majumdar for their important and constructive comments. I give my cordial thanks to Ewen MacDonald for revising the language of the thesis.

I want to thank all co-authors of the publications included in this thesis. I express my sincere thanks to: Jukka Hirvasniemi, Antti Joukainen, Pekko Penttilä, Tuomas Virén, Simo Saarakkala, Heikki Kröger, Petri Lehenkari, Miika T. Nieminen, Erna Kaleva and Panu Kiviranta.

I am deeply grateful to Tuomas Virén, Pia Puhakka and Satu Inkinen for sharing a workroom and having many inspiring discussions. I have been privileged to work in a splendid team. I

would like to thank the BBC-group: Isaac Afara, Antti Aula, Elvis Danso, Chibuzor Eneh, James Fick, Mikko Finnilä, Cristina Florea, Kimmo Halonen, Juuso Honkanen, Mari Huttu, Jarkko Iivarinen, Petro Julkunen, Siru Kaartinen, Janne Karjalainen, Kesämies, Harri Kokkonen, Mikko Lammi, Roope Lasanen, Pauno Lötjönen, Markus Malo, Mika Mononen, Moukku, Janne Mäkelä, Heikki Nieminen, Mikko Nissi, Katariina Nissinen, Simo Ojanen, Xiaowei Ojanen, Jari Rautiainen, Ossi Riekkinen, Ari Ronkainen, Lasse Räsänen, Elli-Noora Salo, Jaakko Sarin, Dmitry Semenov, Tuomo Silvast, Petri Tanska, Matti Timonen, Mikael Turunen, Mikko Venäläinen, Sami Väänänen and Janne Ylärinne. Especially, I want to thank Rami Korhonen for the lessons on his ranch.

I am very grateful for Tarja Holopainen, Pasi Karjalainen, Tero Karjalainen, Sanna Jylhä, Soile Lempinen and Kari Leskinen for the administrative work. Arto Koistinen, Jukka Laakkonen, Mauri Puoskari, Aimo Tiihonen, Virpi Tiitu, Eija Rahunen and Heikki Väisänen have provided valuable technical support and assistance. I also want to acknowledge Tapani Lahtinen and Tero Vatanen. They instructed me on clinical work in hospital. I further want to thank Berliners. Dominik Fachet, Nils Männicke, Martin Schöne and Kay Raum, it has been a pleasure to co-operate with you.

I have been happy to study, teach and discuss physics with wonderful people. I wish to thank Minna Husso, Jani Huttunen, Eerika Häkkinen, Iiro Jantunen, Aki Pajunoja and Jarimatti Valkonen.

I want to thank all my friends Häiskä, Heikki, Olli, Paronin koira, Arppe, Vaimo, Konna-Leena, Konnari, Navigaattori, Venemies, Koistinen, Möykky, Tohtori, Manninen, Konemies, Riina, Niiranen, Nikke, Taneli, Todistaja, Rytkönen, Laulavat arkkitehdit, Jussi, JP, Boothill, Risto, Dosentti, Bravda, Tapsa, Sami, Jarkki, Lena and Romo in Jori's Bar for supporting me through these years, and for giving me opportunities to relax and think other things than research. I owe my deepest thanks to Jani Heikkinen, Sasu and Katriina Kerman, Antti Immonen and Mika Orasmaa for their artwork. They have been feeding my hunger of aesthetics.

Loving thanks to my ideological family: Eeva-Liisa Perki-Latvaniemi, Terttu Vilpponen-Salmela, Sari Raassina, Aku Latvaniemi, Aarre Latvaniemi, Jyrki Katainen, Veijo Tertsunen, Anu Sorjonen, Juho Romakkaniemi, Jussi Ruuskanen, Pirkko-Liisa Piironen and Katriina Kankkunen. They know who I am at my worst and best. Special thanks to my dear friends Wille Berlin, Petri Martikainen and Toni Tuomainen.

Above all I want to express how grateful I am to my parents Arja Isola and Kari Liukkonen as well as my brother Olli-Ville Liukkonen. You provided me a safe and happy childhood in a loving home. Your support has been precious through my life.

Finally, I want to dedicate my heartfelt gratitude to my favorite friend Antonio Carrillo, who has led me to amazing adventures and shown worlds beyond science.

Särkiniemi, March 2015 *Jukka Liukkonen*

This work was supported by the Academy of Finland (projects 132367, 128603, 267551 and 260321), the strategic funding of University of Eastern Finland, Kuopio Univeristy Hospital (EVO, VTR), International Doctoral Programme in Biomedical Engineering and Medical Physics (iBioMEP), North Savo Regional Fund (Hulda Tossavainen foundation), the Magnus Ehrnrooth foundation and the Oskar Öflund foundation.

LIST OF ABBREVIATIONS

2D, 3D	two-dimensional, three-dimensional
CT	computed tomography
diam.	diameter
ECM	extra cellular matrix
FD	finite difference
FDTD	finite difference time domain
FT-IRIS	Fourier transform infrared spectroscopy
GAG	glycosaminoglycan
ICRS	International Cartilage Repair Society
IVUS	intravascular ultrasound
MRI	magnetic resonance imaging
μCT	micro–computed tomography
OA	osteoarthritis
OCD	osteochondritis dissecans
PBS	phosphate-buffered saline
PG	proteoglycan
QUI	quantitative high-frequency ultrasound imaging
SOS	speed of sound
TOF	time-of-flight
X-ray	radiographic imaging

LIST OF SYMBOLS

A	amplitude
$A_{\max}$	maximum amplitude
AIB	apparent integrated backscattering
c	arbitrary constant, wave velocity
c_{P}	specific heat of medium
d_{i}	distance
E	Young's modulus
f	frequency
h	increment, difference
I	intensity, grid index
i	imaginary unit, index number
IRC	integrated reflection coefficient
J	grid index
K	grid index
n	number of samples or patients
m	index number
p	pressure, level of statistical significance
R	reflection coefficient, correlation coefficient
r	correlation coefficient
S	enegy spectra
$sCV(\%)$	standardized coefficient of variation
t	time
$u, u = f(x, y, z, t)$	displacement of single particle as a function of position and time, vibration speed
URI	ultrasound roughness index
$v_{\mathrm{l}},\ v_{\mathrm{t}}$	longitudinal and transversal velocities
x	distance
Z	acoustic impedance

α_s	scattering coefficient
α_{abs}	absorption coefficient
ΔI	intensity difference
ΔA	amplitude difference
$\Delta x, \Delta y, \Delta z$	spatial increments
ϕ	phase difference, bulk viscosity
γ	experimental constant
η	shear viscosity
λ	wavelength, Lamé's first parameter
μ	Lamé's second parameter
θ	angle
ρ	density
ω	angular frequency

LIST OF PUBLICATIONS

This thesis is based on the following original articles, which are referred to in the text by the Roman numerals (I-IV):

I Liukkonen J, Hirvasniemi J, Joukainen A, Penttilä P, Virén T, Saarakkala S, Kröger H, Jurvelin JS, Töyräs J: "Arthroscopic ultrasound technique for simultaneous quantitative assessment of articular cartilage and subchondral bone: an in vitro and in vivo feasibility study", *Ultrasound Med Biol.* **39**, 1460-8, 2013.

II Liukkonen J, Lehenkari P, Hirvasniemi J, Joukainen A, Virén T, Saarakkala S, Nieminen MT, Jurvelin JS, Töyräs J: "Ultrasound arthroscopy of human knee cartilage and subchondral bone in vivo", *Ultrasound Med Biol.* **40**, 2039-47, 2014.

III Kaleva E, Liukkonen J, Töyräs J, Saarakkala S, Kiviranta P, Jurvelin J: "2-D finite difference time domain model of ultrasound reflection from normal and osteoarthritic human articular cartilage surface", *IEEE Trans Ultrason Ferroelectr Freq Control* **57**, 892-9, 2010.

IV Liukkonen J, Jurvelin JS, Töyräs J: "Finite difference model of ultrasound propagation in articular cartilage", submitted.

The thesis also contains previously unpublished data.

AUTHOR'S CONTRIBUTION

The publications presented in this dissertation are original research papers on ultrasound arthoscopy and finite difference modeling of ultrasound propagation in articular cartilage.

In paper **I**, the author carried out the measurements and data analysis, and was the principal author of the manuscript.

In paper **II**, the author conducted the in *vitro* and *in vivo* measurements and analysis. The author was the principal author of the manuscript.

In paper **III**, the author was responsible of the numerical modeling and analysis and contributed to the preparation of the manuscript.

In paper **IV**, the author designed and carried out the numerical simulations, analysed the results and was the principal author of the manuscript.

In all of the papers, the contributions with the co-authors have been significant.

Contents

1 Introduction

Articular cartilage is a highly specialized tissue covering the ends of the articulating bones, shielding them from excessive mechanical stress and friction. Cartilage has nonhomogeneous structure and composition [1–3]. The mechanical properties of articular cartilage are based on structural anisotropy and fibril reinforced poroviscoelasticity. The main components of cartilage are collagen (type II) fibrils, proteoglycan macromolecules (PGs) and water. The interactions between these structural components govern the mechanical response of articular cartilage. It is essential that cartilage retains its structural integrity if it is to maintain its functionality [4].

In the early stages of cartilage degeneration, the compressive stiffness of cartilage decreases as the PG content of superficial tissue is reduced, the water content increases and the organization of collagen fibrils deteriorates [5–7]. Because the cartilage tissue has a limited capability for repair, even minor changes in the structure or composition can lead to a pathogenic condition, osteoarthritis (OA) [5, 8]. OA is the most common joint disease and it has significant socioeconomic consequences [9]. OA causes pain and loss of mobility to millions of people all around the world [8].

In current clinical practice, the diagnosis of OA is based on palpation, and the results of radiography and magnetic resonance imaging (MRI). Unfortunately the early signs of OA are not visible in radiography [10]. MRI suffers from inadequate resolution in its ability to detect signs of incipient OA and furthermore its availability is limited. The current advanced MRI methods for quantifying matrix changes normally require a long acquisition time [11]. In addition, these methods are non-optimal for real-time monitoring of surgical interventions. Often, findings obtained with pre-operative methods such as radiography and MRI need to be verified with arthroscopy. Arthroscopy is also needed to facilitate the surgical repair of cartilage and meniscus injuries.

During arthroscopy, cartilage is evaluated by means of visual inspection and subjective mechanical probing. Unfortunately, the inter-observer reliability of the arthroscopic grading of cartilage lesions is poor [12], and the majority of orthopedic surgeons have indicated that they would prefer more quantitative arthroscopic methods with which to diagnose cartilage lesions more effectively [13]. Thus, better arthroscopic methods capable of quantitative evaluation of articular cartilage would be valuable. These methods could also contribute to the development of novel medical and surgical treatments.

Quantitative high-frequency ultrasound imaging (QUI) has been successfully applied *in vitro* to evaluate several properties of articular cartilage, including surface roughness [14, 15], integrity of the superficial layer [15, 16], state of maturation [17], effects of enzymatic degradation [18, 19], spontaneous repair [20, 21] and tissue thickness [22]. QUI has been also used to evaluate the status of the subchondral bone *in vitro* [16, 23, 24].

Intravascular ultrasound is a clinical high frequency imaging modality originally designed for use during cardiovascular surgery [25]. The technique enables real time, high resolution imaging and, when modified and adapted, it has been shown to have the potential also to assess articular cartilage. In ultrasound arthroscopy, this technique can be exploited to image articular cartilage during conventional arthroscopy. Ultrasound arthroscopy has been used to evaluate cartilage thickness, ultrasound reflection and backscattering [21, 26, 27], and found to provide valuable diagnostic information. However, the clinical feasibility of the ultrasound arthroscopy for simultaneous assessment of articular cartilage and subchondral bone has not been determined. Furthermore, the interpretation of ultrasound data achieved in ultrasound arthroscopies needs to be clarified. In addition a full understanding on the interplay between sound waves and cartilage constituents requires that one applies modeling approach.

The finite difference time domain (FDTD) method has been used to model acoustic wave propagation in inhomogeneous media [28,

29]. It has also been applied successfully to model ultrasound propagation in bone tissue [30–34]. Previously, when evaluating the subchondral bone, the effects of cartilage have not been taken into account or cartilage has been considered as a water-like homogeneous and isotropic tissue.

This thesis focuses on the further investigation and development of the ultrasound arthroscopy technique, and consists of experimental *in vitro* and *in vivo* studies as well as two modeling studies. In experimental studies I and II, feasibility of simultaneous arthroscopic ultrasound assessment of articular cartilage and subchondral bone was investigated. In modeling studies III and IV, numerical models for ultrasound reflection from the articular surface and propagation in cartilage were devised and evaluated.

2 Articular cartilage and subchondral bone

2.1 STRUCTURE AND COMPOSITION OF ARTICULAR CARTILAGE

Collagen is the main structural protein in connective tissues. Collagen, mainly (90-95%) type II collagen, accounts for roughly 10-20% of cartilage wet weight [35] and approximately 60% of its dry weight [6]. The rest of the collagen are types IV, IX, X and XI. Collagen forms fibrils with diameters varying from 20 to 200 nm [35]. The fibrils are cross-linked and form a network architecture [36,37] which confers both high tensile stiffness and strength for the tissue [36–39]. The fraction of collagen of tissue dry weight decreases from superficial to deep cartilage [40].

In Benninghoff's model [1] (Figure 2.1) cartilage is divided into depth-wise zones based on the varying arrangements of the collagen fibrils. In the superficial zone (5-10% of the total thickness [41]), the collagen fibrils are densely packed and arranged in parallel to the articular surface [1,42,43], in this zone their volume density is lowest [44].

In the middle zone (5-20% [41]), the fibrils bend toward the subchodral bone and are randomly oriented [1,45,46]. Here, the collagen volume density is moderate [44].

In the deep zone (70-90% [41]) the collagen volume density is highest [44] and the fibrils are oriented perpendicularly to the articular surface. The fibrils are anchored to the bone through calcified cartilage. Although Benninghoff's model is widely applicable, both anatomical site and species dependent variations in the collagen network organization have been reported [47–50].

Proteoglycans (PGs) are macromolecules accounting for approxi-

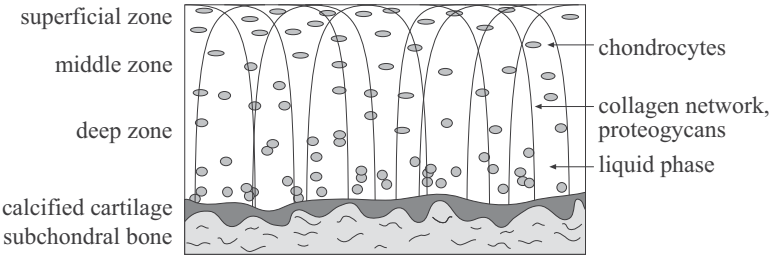

Figure 2.1: Schematic presentation for the structure of articular cartilage.

mately 5-10% of cartilage wet weight [35, 39]. Glycosaminoglycan (GAG) chains, such as chondroitin sulphate and keratin sulphate connected to the core protein are made up of PGs [35]. The PG monomers are bound to a single hyaluronan chain forming a PG aggregate [51, 52]. PG concentration increases from the superficial zone to the deep zone [35, 40, 53]. The negative charge of GAGs attracts sodium ions (Na^+) leading to the formation of osmotic pressure inside cartilage.

Chondrocytes are specialized cells (diam. $\approx$ 15 μm) responsible for manufacturing and maintaining the extracellular matrix (ECM). Chondrocytes make up roughly 1-5% of the cartilage volume [54,55] and less than 5% of cartilage wet weight [35]. In the superficial, the zone chondrocytes are small, flat and oriented tangentially to the articular surface [46, 56]. In the middle zone, the chondrocytes are of medium size and spherical [46,56]. In the deep zone, one encounters the largest chondrocytes, they are arranged in vertical columns and metabolically they are most active [46, 56, 57]. The mechanical and chemical environments, *e.g.*, external stress and fluid flow affect the function of chondrocytes [6, 54, 58].

Interstitial water containing electrolytes contributes about 60-80% to the cartilage wet weight [40, 51]. Although some water is bound in chondrocytes and collagen fibrils, most of the water is free [59]. The flow of free water plays an important role in determining the mechanical properties of articular cartilage [35] as well as providing lubrication of the articulating surfaces. The convection of water and

its diffusion provide nutrition and allow the exchange of ions in cartilage [35, 60]. The water content decreases from the superficial zone towards the deep zone [61, 62].

2.2 FUNCTION OF ARTICULAR CARTILAGE

In ECM of articular cartilage, the PG macromolecules are bound in the tissue by the collagen network. The negative charge of GAGs produces repulsive forces which expand the ECM. Furthermore, the tissues swells due the osmotic pressure caused by negatively charged GAGs as they attract Na^+-ions and the increase in the total inorganic ion concentration and the resulting elevated osmolarity. The swelling is resisted by the collagen network. The diverse interplay between the components of porous viscoelastic anisotropic tissue explains the behavior of articular cartilage during mechanical loading. [39, 63, 64] The viscoelasticity leads to time-dependent properties that can be divided into flow-dependent and flow-independent parts. The flow-dependency is described by the frictional flow of the interstitial fluid [65]. In contrast, the flow-independent time-dependent behavior is associated with intrinsic viscoelasticity of the collagen and PG-matrix [66].

When a constant compressive force is applied onto an articular surface, it causes the fluid to flow within and out of the porous tissue. The low permeability of the extracellular matrix prevents any rapid escape of interstitial fluid. At mechanical equilibrium, the fluid flow will cease and the resistance to the compressive force is mainly caused by the solid matrix [67–69]. As the compression ends, fluid flows back into tissue and it regains its original volume. During static loading, a hyaluronate binding protein, lubricin, which is present in synovial fluid and at the cartilage surface helps to lubricate the surface of cartilage [60].

Under an instantaneous compressive load, the fluid flow plays a minor role in the mechanical response. As the interstitial fluid has no time to escape from the tissue it becomes pressurized and carries the applied load [70–72]. The permeability of articular car-

tilage is small (approximately 10^{-16} $m^4 \cdot N^{-1} \cdot s$) [73]. In a confined compression test of articular cartilage, it has been shown that the interstitial fluid provides more than 95% of the total load support [74]. For intact articular cartilage, this high percentage of fluid load support can last more than 500 s [73]. In addition, the collagen network contributes to load bearing by resisting the deformation of cartilage [75–77]. In dynamic loading, the articular surface is lubricated mainly by the interstitial water as it is pressurized and flows through the cartilage surface [78].

2.3 OSTEOARTHRITIS AND CARTILAGE LESIONS

Osteoarthritis is a holistic joint disease involving the degeneration of articular cartilage and catabolic changes in other joint tissues. OA is the one of the most common reasons for mobility problems not only in senior citizens but also in people of working age.

2.3.1 Etiology

The development of OA is not fully understood [79]. Often OA develops along with aging without any specific reason (primary OA). In addition, OA can be initiated after an injury, infection or dislocation (secondary OA). [6,7,80] Cartilage has a limited ability to recover. When chondrocytes detect degenerative changes in tissue, they start a restoration process, *i.e.*, synthesis of collagen and PGs [7,81]. If the degradation process of cartilage overwhelms the chondrocytic response, OA passes a point of no return [35]. The loss of PGs has been reported to be reversible, but the disruption of the collagen network is believed to be irreversible [82–85].

The first signs of OA are fibrillation of collagen network and the loss of PGs [5,6,86]. These changes lead to an increase in the permeability and water content. As a result, the tissue swells and becomes softer. At the same time fissures in the articular surface may occur [7]. In the next phase of OA, cartilage becomes thinner, the tissue tears and fragments of cartilage end up in the joint space.

Finally, the underlying subchondral bone is revealed, evoking pain in articulating bones and the joint becomes dysfunctional or even immobile [6,87].

2.3.2 Diagnostics

Clinically, OA is diagnosed based on the results of the physical examination and the severity of symptoms such as tenderness, swelling, reduced movement or instability of the joint [88,89]. The diagnosis may be confirmed by X-ray or magnetic resonance imaging (MRI). Advanced OA can be detected radiographically as a narrowed joint space or alterations in the subchondral bone [90]. Unfortunately the almost identical attenuation in articular cartilage and surrounding tissues limits the visibility of cartilage in X-ray and computed tomography (CT) images. Thus, the early stages of OA cannot be revealed [10]. MRI makes it possible to assess the cartilage thickness, lesions and alterations in subchondral bone and meniscus [91]. However, high costs, long acquisition times and limited resolution (size detection limit of 200 μm with a 9.4 T experimental system [92]) limit the use of current MRI devices in the diagnostics of incipient OA. In addition, the intra-observer reliability of the MRI grading has been reported to be poor [93].

Arthroscopy is an invasive type of joint assessment technique, enabling a visual evaluation and mechanical probing of the articular surfaces. Its invasiveness limits its use in diagnostics of OA, but it is widely applied in the evaluation of the scoring of cartilage lesions [13]. The international Cartilage Repair Society's (ICRS) scoring system can be used to classify the lesions by dividing cartilage integrity into five categories: intact (0), nearly normal (1), abnormal (2) and severely abnormal (3 and 4) [94]. The categories are described by the depth of the lesion, the integrity of the articular surface and the stiffness of cartilage [94]. Nonetheless, the arthroscopic evaluation is subjective and poor intra- and inter-rater agreements have been reported [13,95]. At the same time, the majority of even experienced arthroscopists have been reported to feel unsure of the

grading and thus there is a clear demand for measurement devices that would provide an objective cartilage grading [95].

2.3.3 Treatment

At present there is no curative treatment available for OA. However, symptomatic treatments providing pain relief and maintenance of mobility are available. Physical or occupational therapy may also be utilized. Commonly these include a loss of excess weight, muscle strengthening, ergonomic improvements, motion exercises and patient education. When chronic pain occurs or mobility and daily activities become difficult, pharmacological treatment or surgery may be considered [96–99].

The pharmaceutical approach consists of analgesics, nonsteroidal anti-inflammatory drugs or intra-articular injections of hyaluronic acid or glucocorticoids [96]. At best, even the injections provide only a short-term pain relief for up to six months [96]. In addition, their many side effects have limited the prolonged use of nonsteroidal anti-inflammatory drugs [96,100,101]. Disease-modifying drugs and intra-articular drug delivery systems are under development [102], *e.g.*, non-invasive ultrasonic delivery of therapeutic compounds has been reported to be a promising technique available in the immediate future [103].

The most common surgical procedures for repair of cartilage injuries are microfracturing [97,104,105], autologous chondrocyte transplantation [98] and osteochondral mosaicplasty [106]. In the microfracturing procedure, the articular cartilage over the lesion area is removed and the subchondral bone is perforated with many holes [104,105] which allow the mesenchymal cells to leave the bone marrow and to gain access to the surface of the subchondral bone. The cells differentiate into fibrous chondrocytes forming fibrocartilage in the lesion area [97]. Unfortunately, the fibrocartilage and hyaline cartilage differ in both structure and composition, *e.g.*, fibrocartilage has less type II collagen. The recovery is only temporary as the clinical benefits have been reported to deteriorate with

time [105].

In autologous osteochondral transplantation, small cylindrical osteochondral plugs from the non-weight bearing locations are transplanted into the lesion area [107]. This can be conducted during a single operation. The results of the autologous mosaicplasty treatments have been encouraging [97]. The operation is feasible only if the lesion site is relatively small and suitable donor sites can be found. In addition, the results may suffer from the differences in the structure and composition between the transplant and the surrounding tissue.

Autologous chondrocyte transplantation is conducted in two phases. In the first phase, chondrocytes are harvested from low weight bearing sites of a joint for culturing. In the second phase, the cultured cells are injected in the lesion area and covered with a periosteal graft [108]. Autologous chondrocyte transplantation may result in hyaline cartilage appearing the lesion area [108]. However, the technique is time consuming [97] and the harvesting of the periosteal grafts may lead to complications [99].

The total joint replacement is the ultimate surgical operation, suitable when the other treatments are insufficient or inapplicable. Approximately 90% of the patients are satisfied with the results of the operation [109]. Unfortunately, the cost of the surgery is high and sometimes a revision operation is needed [109].

2.4 SUBCHONDRAL BONE

Subchondral bone is located immediately under articular cartilage and provides support for it. The abnormal interplay between articular cartilage and subchondral bone is an essential component in the development of OA. Increases in the thickness and density of subchondral bone and formation of cysts are often associated with OA [6, 7, 110]. It has been postulated that OA development originates from subchondral bone [110–112]. Putatively, the dyssynchrony in the adaptation of the cartilage and bone disrupts the physiological relationship between the articular cartilage and sub-

chondral bone and contributes to OA pathology [110]. Even though the fundamental cause of OA remains unclear, it is evident that a simultaneous diagnostic assessment of articular cartilage and subchondral bone would greatly contribute to the early detection of OA. Furthermore, surgical treatments involving operations in subchondral bone, *e.g.*, osteochondral autograft could benefit if there had been a prior assessment of the health of the subchondral bone.

3 Ultrasound

3.1 BASICS OF ULTRASOUND

Ultrasound is a mechanical wave motion beyond the audible limit of 20 kHz. Practically the upper limit for ultrasound frequency in liquids is around 500 MHz due to the extensive attenuation (equation 3.15). In this presentation, the propagation of ultrasound in homogeneous, elastic and isotropic medium will be described. The ultrasonic propagation can be differentiated into two different types of plane waves: transverse and longitudinal. A transverse or shear wave is formed when the oscillation of the particles is perpendicular to the direction of the wave propagation. Shear waves do not occur in low-viscous medium such as air or water [113]. In articular cartilage, the shear waves play only a minor role [114, 115]. When the particles vibrate in parallel to the direction of the wave propagation, a longitudinal or pressure wave is formed.

The linear wave equation [116]

$$\frac{\partial^2 u}{\partial x^2} = \frac{1}{c^2}\frac{\partial^2 u}{\partial t^2}, \tag{3.1}$$

describes the displacement ($u = f(x,t)$) of single particle as a function of distance (x) and time (t). The solutions for the partial differential equation (3.1) take the form

$$u(x,t) = u_1(ct - x) + u_2(ct + x), \tag{3.2}$$

with suitable functions u_1 and u_2. In acoustics, the most commonly used expression is $e^{i\omega(t \pm x/c)}$ or the corresponding trigonometric expression. Solutions are critically dependent on the selected initial and boundary conditions. These conditions are usually selected by investigating the system in specific time points and locations, *i.e.*, interfaces of the medium to meet the requirements of the system in known states.

In an elastic medium, a multidimensional wave can be represented with a one dimensional wave equation provided that excessive medium is assumed; so that the effects of the boundaries can be neglected. In this case, the boundary conditions are similar in each point and the wave magnitudes are a function of distance parallel to the normal of the planar waves. In this case, the real part of the function u_1 (3.1) gives the pressure amplitude (A):

$$A = A_{\max} \cos(\omega_0 t + \phi), \tag{3.3}$$

where $A_{\max}$ is the maximum amplitude of the wave, ω_0 is the angular frequency, t is time and ϕ is the phase difference [117]. The velocity and acceleration related to A are the derivatives of the equation (3.3). The propagating wave is formed when the particles undergo one by one the harmonic movement. The velocity of propagating wave is given by the equation

$$c = f\lambda, \tag{3.4}$$

where f is the frequency and λ is the wavelength. In practice, the density and elastical properties of the medium affect the speed [113]. The average speed of sound in human soft tissues has been reported to be approximately 1550 m/s [118].

Intensity I is defined with ρ, c and u by the equation

$$I = \frac{1}{2}\rho c u^2. \tag{3.5}$$

The comparison of ultrasound intensities is usually conducted on the decibel-scale:

$$\Delta I = 10 \log_{10} \frac{I}{I_0}, \tag{3.6}$$

where I is the measured intensity and I_0 is the reference value. The amplitudes A and A_0 can be compared similarly using the equation

$$\Delta A = 20 \log_{10} \frac{A}{A_0}. \tag{3.7}$$

If no attenuation is assumed the pressure of the propagating wave is directly proportional to the density ρ, propagation speed c and vibration speed u [113]

$$p = \rho c u. \tag{3.8}$$

Acoustic impedance Z is a fundamental magnitude defined as a product of the density ρ and velocity c

$$Z = \rho c. \tag{3.9}$$

In human soft tissues, acoustic impedance is approximately the same as in water ($1.6 \cdot 10^6$ Pa $\cdot$ s/m) [118].

Absorption In practice, acoustic systems are neither elastic nor homogeneous. In these cases, the energy of the propagating wave is transferred to heat energy absorbed by the medium either directly or indirectly. The conventional absorption coefficient is defined as the sum of viscous and thermal attenuation by the equation

$$\alpha_{\text{abs}} = \frac{\omega^2}{2\rho_0 c^3} \left(\frac{4}{3}\eta + \frac{(\gamma - 1)\kappa}{c_{\text{P}}} \right), \tag{3.10}$$

where ω is the angular frequency, ρ is the density, η is the viscosity, γ is an experimental constant ja c_{P} is the specific heat of the medium [117]. By assuming that it is an adiabatic and isothermal process ($\gamma \longrightarrow 1$), the absorption can be described by the equation

$$\alpha_{\text{abs}} = \frac{8\pi^2 f^2 \eta}{3\rho c^3}, \tag{3.11}$$

where f is the frequency, η ja ρ are the viscosity and density of the medium respectively and c is the speed of sound in the medium [117].

In soft tissues, the overall absorption has been described as the sum of four components: relaxation processes, relative movement,

bubble mechanisms and hysteresis [113,119]. In the relaxation process, a temporal density change in the medium increases its internal energy but only part of the energy is transformed back to the energy of the propagating wave. When relative motion occurs, the internal structures of medium such as cells are moved by the wave front and the wave loses the corresponding energy. The bubble mechanisms contribute a part of the wave energy to the micro bubbles in the medium. The energy loss in hysteresis is due to the non-linearity between the compression and compressive forces.

Scattering, refraction and reflection When a propagating wave arrives at the interface between two materials with different acoustic impedances reflection, refraction and scattering may occur. Reflection and refraction typically occur when the target is significantly larger than the wavelength. The boundary condition of the wave equation (3.1) is a continuation of the pressure in the interface. This is governed by Snell's law

$$\frac{\sin\theta_i}{c_i} = \frac{\sin\theta_t}{c_t}, \tag{3.12}$$

where θ_i and c_i are the angle and velocity of the arriving wave respectively, and θ_t and c_t the angle and velocity of the refracting wave respectively. The angle θ_r of the reflected wave is the same in size with θ_i and line symmetric with respect to the normal of the reflecting interface. In an isotropic solid material, Snell's law must be applied separately to the longitudinal and transversal components [120].

When particle velocity with respect to the normal of the reflective interface is assumed to be continuous, the relationship between pressures of the reflected (p_r) and incident (p_i) waves is obtained as a reflection coefficient

$$R_\mathrm{amp} = \frac{p_\mathrm{r}}{p_i} = \frac{Z_2\cos\theta_\mathrm{i} - Z_1\cos\theta_\mathrm{t}}{Z_2\cos\theta_\mathrm{i} + Z_1\cos\theta_\mathrm{t}}. \tag{3.13}$$

Here θ_i and θ_r are the angles of arrival and refraction respectively and Z_1 and Z_2 are the acoustic impedances of the interfacing

mediums. The reflection coefficient of sound wave intensity (R_{int}) is the square of R_{amp}; R_{int}=R_{amp}^2 [117].

When the target is the same as size as the wavelength or smaller, then scattering may occur. In scattering phenomenon, the direction of the propagating wave changes and the plane waves spread locally. The scattering properties of materials are described with the scattering coefficient α_{s} which depends on frequency.

The overall attenuation can be expressed as a sum of the abovementioned processes with the equation

$$\alpha(f) = \alpha_{\text{abs}}(f) + \alpha_{\text{s}}(f), \tag{3.14}$$

where $\alpha_{\text{abs}}(f)$ and $\alpha_{\text{s}}(f)$ are specific frequency dependent coefficients for the medium. Usually, in soft tissues, the equation

$$\alpha(f) = \alpha_0 f^y, \tag{3.15}$$

is valid. Here α_0 and y are experimentally determined constants. Typically $(0 < y \leq 2)$ [121].

3.2 GENERATION OF ULTRASOUND

Ultrasound waves can be created by several techniques: magnetostrictive [122–124], electrostatic [125, 126], capacitive [127] and piezoelectric [128] devices have been developed. Joule [122] observed the magnetostriction effect, *i.e.*, a change in length occurs in a rod of a ferromagnetic substance such as nickel, when a magnetic field is applied along its length. In an electrostatic transducer, a dielectric foil vibrates between the electrodes due the electrostatic forces [126]. The capacitive ultrasonic technique is an old concept but only recent advances in microfabrication technology have made it possible to build practical capacitive ultrasound transducers that can compete with their piezoelectric counterparts [127]. In a capacitive ultrasonic transducer, a single element consists of numerous capacitor cells made from a metalized membrane and a silicon substrate. When it is being used, an alternating voltage is applied

between the metalized membrane and the substrate to generate ultrasound. In medical applications, the most common way to generate ultrasound is to exploit the piezoelectric phenomenon [118,128] which is presented in the following section.

Piezoelectric Transducer In a direct piezoelectric effect, a piezoelectric material builds up a charge on its surface when mechanical stress is applied. In the opposite phenomenon, the indirect piezoelectric effect, material undergoes mechanical deformation in an electric field. [113, 118]. The reversible nature of piezoelectric materials enables their use as a source and receiver of ultrasound. In transmission the piezoelectric material is driven by the applied voltage, while when receiving the electrical pulses produced by the material are acquired.

In a simple flat (non-focused) ultrasound transducer, the piezoelectric material is commonly located between a backing material and a matching layer. The backing material is selected to absorb ultrasound pulses propagating in a backward direction. The purpose of the matching layer is to minimize the ultrasound interactions such as reflection between the piezoelement and the medium. [118] A focused ultrasound transducer can be constructed by shaping the piezoelement, adding an acoustic lens between the piezoelement and medium or by use the of the phased array technique. Focusing improves the lateral resolution of ultrasound and directs the ultrasound energy in a specific location. In the phased array technique, the transducer includes several piezoelements and time delays are regulated by selected electrical pulses. In contrast, when using a concave piezoelement or an acoustic lens, this method allows focusing at different depths. The phased array technique is the most commonly used focusing arrangement in medical ultrasonics.

3.3 ULTRASOUND IMAGING

In ultrasound imaging, the pulse-echo method is the most common method. In this geometry, the same transducer acts as the transmit-

ter and the receiver. With a phased ultrasound array, an ultrasound image is constructed by collecting ultrasound signals from each element. The conventional 2D ultrasound image contains the lateral locations in the x-axis, the depth or time of flight information in the y-axis and the colors represent the amplitudes at the each location.

The spatial resolution of any imaging system is defined as its ability to distinguish two points as being separate in space. The resolution of the ultrasound image must be defined separately for the axial and lateral dimensions. The axial resolution is the resolution in the direction parallel to the ultrasound beam; it is the shortest distance between two separate targets in this direction that can be separated. The length and frequency content of the ultrasound pulse determine the axial resolution as a half of the length of the pulse. The frequency dependency of ultrasound attenuation demands that one needs to make a compromise between the axial resolution and imaging depth. The lateral resolution is determined by the dimensions of the ultrasound field and this may change as a function of distance.

3.4 ULTRASOUND ASSESSMENT OF ARTICULAR CARTILAGE

Speed of sound For human and bovine articular cartilage, SOS values between 1580-1760 m/s have been reported [18,19,129–131]. Maturation, anatomical location and integrity affect the speed of sound in cartilage [17,18,132,133]. SOS has been reported to decrease when the collagen [129,134,135] or PG [18,135,136] contents are reduced. In addition, SOS is highest when the ultrasound beam is parallel to the orientation of collagen fibrils [137,138]. When the water content increases, SOS declines [134,135]. In degenerated cartilage, SOS values in the range of 1550-1660 m/s have been reported [18,19,22,129,131].

Reflection Chérin *et al.* have shown that when 1) frequency independency, 2) perpendicularity between ultrasound beam and cartilage surface, 3) distance long enough from the transducer to the

surface and 4) small dimensions of the surface are assumed, then the reflection coefficient of linear system in the frequency domain can be calculated from the equation

$$R_c = \frac{S_c(z,f)}{S_r(z,f)}, \tag{3.16}$$

where $S_c(z,f)$ and $S_r(z,f)$ are the reflected signals in the frequency domain from the cartilage surface and a perfect reflector, respectively. [139] Typically $S_c(z,f)$ and $S_r(z,f)$ are determined by means of the fast Fourier transform. Chérin's approach is beneficial as the effects of the attenuation, diffraction and characteristics of the measurement system can all be neglected.

In the dB-scale, the energy reflection coefficient is defined as

$$R_c^{\mathrm{dB}}(f) = 10 \cdot \log_{10} \left\langle |R_c(f)|^2 \right\rangle, \tag{3.17}$$

where $\langle \ldots \rangle$ is the mean over all scan lines of the ultrasound image.

For cartilage, the reflection is often quantified with the integrated reflection coefficient (IRC) as follows

$$IRC = \frac{1}{\Delta f} \int_{\Delta f} R_c dB(f) df, \tag{3.18}$$

where Δf refers to the -6 dB frequency bandwidth. In addition, the reflection coefficient in the time domain is often applied in the literature. With the previous assumptions, this can be calculated as follows

$$R_c = \frac{A_c}{A_r} \cdot 100, \tag{3.19}$$

where A_c and A_r are the peak-to-peak amplitudes of the signals reflected from cartilage and perfect reflector, respectively.

In OA, the surface roughness and water content of cartilage increase and the collagen content declines. This leads to a decrease in the reflection at cartilage surface. In bovine cartilage, it has been

reported that there is a notable difference in the reflection coefficient between the intact ($IRC \approx -27$ dB, $R \approx 5\%$) and degenerated ($IRC \approx -34$ dB, $R \approx 2\%$) [16].

Backscattering Chérin *et al.* introduced a method for the quantification of backscattering in cartilage. The backscattered energy is defined as follows

$$\mu_c = \frac{S_B(z,f)}{S_r(z,f)}, \tag{3.20}$$

where $S_B(z,f)$ and $S_r(z,f)$ are the energy spectra of the scattered sound from cartilage and reflected sound from the perfect reflector, respectively [139]. The apparent integrated reflection coefficient (AIB) in the dB-scale is defined with the equation

$$AIB = \frac{1}{\Delta f}\int_{\Delta f} \mu_c dB(f) df, \tag{3.21}$$

where Δf indicates the -6 dB frequency bandwidth of the ultrasound transducer.

Attenuation The ultrasound attenuation is related to the composition and structure of the cartilage [69] and the integrity of the collagen cross-links [140]. Ultrasound attenuation has been reported to decrease along with spontaneous degeneration as more and more collagen and PGs become affected [131]. A wide range for ultrasound attenuation values has been reported at different frequencies 1.8-2.7 dB/mm (5-9 MHz) [131], 2.8-6.5 dB/mm (10-40 MHz) [141] and 92-147 dB/mm (100 MHz) [140]. This agrees with the frequency dependency of attenuation as stated in the equation (3.15).

Ultrasound roughness index Saarakkala *et al.* have introduced the ultrasound roughness index (URI) as a quantitative measure of the microroughness of the articular surface. When perpendicularity between ultrasound beam and cartilage is assumed, URI is defined as follows

$$URI = \sqrt{\frac{1}{m}\sum_{\mathrm{i}=1}^{m}(d_{\mathrm{i}} - \langle d \rangle)^2}, \tag{3.22}$$

where m is the number of the measurement points, d_i is the distance between the cartilage surface and the ultrasound transducer at each measurement point and $\langle d \rangle$ is the average distance [142]. In case of non-perpendicularity, trend removal techniques can be applied [142]. URI values of 7.4 ± 1.2 μm have been reported for intact cartilage, whereas much higher values (24.4 ± 15.5 μm) are found in degenerated cartilage [16].

4 Modeling of ultrasound propagation

The propagation of ultrasonic waves can be studied analytically or numerically although these approaches may also be combined. In the analytical approach, a set of acoustical equations, *e.g.*, the constitutive wave equation and Snell's law, are utilized. Modeling is carried out by solving these equations at each point of interest. The better the selected equations cover the interactions in the modeled space, the better will be the analytical results. In order to create a realistic model of ultrasound propagation many factors for example anisotropy, heterogeneity, non-planarity, attenuation and arbitrary shaped pulses should be implemented. In complicated situations, the set of equations increases and extensive computing resources are needed. Thus, the analytical approach provides no solutions for realistic models, making numerical methods necessary. One widely used method is the finite difference (FD) method which can handle relatively complex geometries with reasonable accuracy in a time efficient manner. Furthermore, the FD algorithms are suitable for parallelization.

The FD methods are one of several domain methods along with finite-element, spectral element and pseudospectral methods [143]. These are less accurate compared to boundary methods that solve integral forms, but advantageous in terms of efficiency [144]. In the FD method, a set of discrete points in space and time form a space-time grid in the computational domain. At each grid point, the values of the functions representing the wave field and the material properties of the medium are studied. FD formulae are applied to achieve approximations for the spatial and time derivatives of the functions in a given position. These formulae define the expression of the derivatives in terms of function values in the grid points

in the neighborhood. Whereas the analytical approach is based on differential equations, the FD method replaces the differential equations with a system of discrete algebraic equations. Three fundamental requirements can be demanded from an FD system: consistency, stability and convergence. The consistency ensures that the original differential equations and difference equations are congruent. The stability means that the error caused by a small perturbation in the numerical solution is bounded. Convergence requires that the finite-difference solution approaches the solution of the original partial differential equation as the increments in space and time approach zero. The FD method can be applied either in the time or the frequency domain [145, 146] although usually, the time domain formulation is utilized since it is more efficient. The fundamental theory for the FD method was established in 1928 by Courant *et al* [147]. The method has been under active investigation since the 1960's [148–151]. The development of the FD methods has escalated in conjunction with the increase in computational power.

4.1 FINITE DIFFERENCE TIME DOMAIN METHOD (FDTD)

The acronym FDTD was introduced by Taflove in 1980 [152]. Before that, the FDTD method was used to solve various physical problems. A remarkable improvement occured with the discovery of the solutions for Maxwell's curl equations [153] on grids staggered in space and time [149]. Maxwell's equations are partial differential equations that govern the relationship between electric and magnetic fields. The superb versatilibity of the Maxwell's equations allows the electric and magnetic fields to be replaced with the stress and particle velocity fields [120] enabling acoustic modeling. An exhaustive presentation is provided in the book written by Auld [120].

The space to be modeled should be covered with a computational domain (a space-time grid) in four-dimensional (x, y, z, t) space, where the variables x, y, z refer to Cartesian coordinates and t is time. Consider a set of discrete points (z_I, y_J, z_K, t_m) given by $x_I = x_0 + I\Delta x$, $y_J = y_0 + J\Delta y$, $z_K = z_0 + K\Delta Z$, $t_m = t_0 +, \Delta t$,

where $I, J, K, m = 0, 1, 2, \ldots$, $\Delta x, \Delta y, \Delta z$ are the spatial increments and Δt is the time step. Often an isotropic spatial grid is used, $\Delta x = \Delta y = \Delta z = h$. The FDTD method approximates a function $u(I, J, K, m)$ at a grid position (x_I, y_J, z_K, t_m) with a grid function $U(x_I, y_I, z_K, t_m)$.

If one assumes function $f(x)$ to have a continuous first derivative. The forward difference

$$\frac{\mathrm{d}f}{\mathrm{d}x}(x_0) = \frac{f(x_0 + h) - f(x_0)}{h}, \tag{4.1}$$

the backward difference

$$\frac{\mathrm{d}f}{\mathrm{d}x}(x_0) = \frac{f(x_0) - f(x_0 - h)}{h} \tag{4.2}$$

and the central difference

$$\frac{\mathrm{d}f}{\mathrm{d}x}(x_0) = \frac{f(x_0 + h) - f(x_0 - h)}{2h} \tag{4.3}$$

are different approximations for the derivative of function $f(x_0)$. Truncation errors can be investigated by substituting the corresponding Taylor expansions for $f(x_0 \pm h)$ in equations (4.1), (4.2) and (4.3). In equations (4.1) and (4.2) the truncation errors are proportional to h. Thus, the equations (4.1) and (4.2) are first-order approximations to the first derivative. In addition, the equation (4.3) provides a second-order approximation as the truncation error is proportional to h^2. Further, a commonly used second-order approximation to the second derivative is

$$\frac{\mathrm{d}^2 f}{\mathrm{d}x^2}(x_0) = \frac{f(x_0 - h) - 2f(x_0) + f(x_0 + h)}{h^2}. \tag{4.4}$$

Consistency, stability, convergency An FD scheme is consistent if the corresponding truncation error, *i.e.*, the difference between partial differential equation and its difference approximation vanishes when $\Delta t \longrightarrow 0$ or $\Delta h \longrightarrow 0$. If this is true only when a certain relationship between Δt and h is met, then the FD scheme is conditionally consistent. An FD scheme is stable if it gives a bounded solu-

tion when the exact solution is bounded. The von Neuman method is the most commonly used method for stability analysis [150]. An FD scheme is convergent if $U(x_I, y_I, z_K, t_m) \longrightarrow u(I, J, K, m)$ when $\Delta t \longrightarrow 0$, $\Delta h \longrightarrow 0$.

Explicity and implicity In an explicit FD scheme, the motion at any spatial grid point can be updated for the next time step using an explicit FD formula which uses only values of motion at previous time steps. In the case of an implicit scheme, there is no explicit formula for updating motion only in one grid point. In an implicit scheme, the motion at a given time level is calculated simultaneously at all spatial grid points from the motion values at previous time levels. The explicit schemes are computationally simpler but they are less accurate and may be unstable.

4.2 VISCOELASTIC WAVE EQUATION IN THE TIME DOMAIN

In homogeneous, isotropic and elastic solids, the ultrasound propagation can be described by the wave equation

$$\rho \frac{\partial^2 u}{\partial^2 t} = \mu \nabla^2 u + (\lambda + \mu) \nabla (\nabla \cdot u), \tag{4.5}$$

where ∇ is the gradient operator, $\nabla\cdot$ is the divergence operator, ∂ is the partial differential operator, $u(x, y, z, t)$ is a displacement vector, t is time, ρ is density and elasticity of the medium is described by Lamé constants λ and μ [154]. The Lamé constants can be expressed in terms of other elastic parameters *i.e.* Young's modulus E and Poisson's ν ratio, that is, $\lambda = \frac{E\nu}{(1+\nu)(1-2\nu)}$ and $\mu = \frac{E}{(2(1+\nu))}$. The viscous losses can be implemented by use of the shear η and bulk ϕ viscosities [155]:

$$\mu \longrightarrow \mu + \eta \frac{\partial}{\partial t} \text{ and } \lambda \longrightarrow \lambda + \left(\phi - \frac{2}{3}\eta \right) \frac{\partial}{\partial t}. \tag{4.6}$$

Substitution of equation (4.6) into equation (4.5) provides the viscoelastic presentation

$$\rho \frac{\partial^2 u}{\partial^2 t} = \left[\mu + \eta \frac{\partial}{\partial t} \right] \nabla^2 u + \left[\lambda + \mu + \phi \frac{\partial}{\partial t} + \frac{\eta}{3} \frac{\partial}{\partial t} \right] \nabla (\nabla \cdot u). \quad (4.7)$$

An explicit FDTD solution for equation (4.7) with the use of a forward difference approximation in time and central difference approximation in space is provided in the publication of Delsanto *et al* [156].

5 Aims of the thesis

Quantitative methods for arthroscopic evaluation of cartilage and subchondral bone are mostly lacking. The ultrasonic assessment of articular cartilage and bone has shown potential in being able to evaluate degenerative and traumatic changes. It was hypothesized that ultrasound arthroscopy could produce diagnostic information would be supplementary to the information provided by conventional arthroscopy. Since cartilage is a highly anisotropic, heterogeneous and multiphasic tissue, its interaction with ultrasound is complex. Therefore, it was hypothesized that numerical models for ultrasound propagation in the articular cartilage would improve the interpretation of the experimental data.

The specific aims for this thesis were:

- To investigate the feasibility of using ultrasound arhroscopy in the simultaneous assessment of articular cartilage and subchondral bone.
- To conduct ICRS grading using ultrasound imaging and to compare the outcome with ICRS grading of visual inspection.
- To investigate numerically ultrasound reflection from articular cartilage with varying surface roughnesses, material parameters (Young's modulus, density, longitudinal, and transversal velocities) and different inclinations of the samples.
- To construct and evaluate a sample specific FDTD model of articular cartilage containing chondrocytes, proteoglycans, collagen and water.

6 Materials and methods

This thesis consists of four independent studies (I-IV). The materials and methods used in the studies are summarized in Table 6.1. The mechanical (study I), histological (study I), microscopy (study I) biochemical (studies I and IV), μCT-imaging (study I) and ultrasound (studies III and IV) data have been obtained from earlier studies [135, 157–160]. The rest of the data is original. The ultrasound data used in study III has been analyzed from a different and novel perspective.

Table 6.1: Summary of materials and methods used in studies I-IV.

Study	Species and tissue	Number of samples or patients	Methods
I	Human cartilage and bone *in vitro*	n=13	Ultrasound imaging Mechanical testing Histological analyses FT-IRIS μCT-imaging
	Human cartilage and bone *in vivo*	n=2	Ultrasound arthroscopy
II	Human cartilage and bone *in vivo*	n=11	Ultrasound arthroscopy Pre-operative CT arthrography
III	Human cartilage	n=43	Ultrasound imaging Light microscopy FDTD-modeling
IV	Bovine cartilage	n=28	Ultrasound, contact technique Light microscopy FT-IRIS Biochemical analyses FDTD-modeling

6.1 SAMPLE PREPARATION AND PROCESSING

In studies I and III human and in study IV bovine osteochondral samples were used. After sample preparation, the osteochondral plugs were immersed in phosphate-buffered saline (PBS) containing enzyme inhibitors (ethylenediaminetetraacetic acid dihydrate and benzamidine HCl) and then frozen. In the *in vitro* experiments, the samples were thawed and immersed in PBS supplemented with inhibitors of proteolytic enzymes throughout the studies. In all studies, the adjacent surrounding tissue was used for reference analyses.

In study I, cylindrical osteochondral specimens (diam.=16 mm, n=13) were drilled from the femoral medial condyles of human cadavers (24–76 years of age) with no history of joint diseases [157].

In study III, patellae (n=14) from the right knees of the cadaveric donors (27-79 years of age) were studied [160]. Six measurement sites on each patella were selected. The corresponding histological sections were prepared, allowing the creation of sample-specific models with realistic surface profiles.

In study IV, bovine patellae were studied [135]. Bovine knee joints were opened and the lateral facets of patellae were visually classified into four degenerative stages: healthy cartilage surface (n=13), smooth but slightly discolored surface (n=5), superficial cartilage defect (n=6) and deep cartilage defect (n=8). Cylindrical (diam.=19 mm) osteochondral plugs were drilled from the predetermined site of the patella. In the acoustic measurements, cylindrical (diam.=4 mm) full-thickness cartilage samples (n=32) were prepared from the center of the osteochondral plug.

6.2 MEASUREMENTS WITH THE ARTHROSCOPIC ULTRASOUND SYSTEM *IN VITRO*

In study I, the samples were degassed for 40 minutes at room temperature before the ultrasound measurements. The ultrasound measurements were conducted using a clinical high-frequency in-

travascular ultrasound (IVUS) device (ClearView Ultra, Boston Scientific, San Jose, CA, USA), equipped with an ultrasound catheter (diam.=2.8 mm, 9 MHz, 26-dB bandwidth 7.1–11.0 MHz).

The intravascular ultrasound radiofrequency signals were recorded and digitized at a sampling frequency of 250 MHz and resolution of 8 bits using a digital oscilloscope (LeCroy, Chestnut Ridge, NY, USA). The signals were stored for off-line analysis using custom-made LabVIEW software (Version 8.2, National Instruments, Austin, TX, USA). The angle between the ultrasound catheter and the cartilage surface was adjusted manually in order to achieve the maximum surface reflection. Data from 10 full rotations of the ultrasound probe were obtained in every measurement. All measurements were repeated three times. The catheter was removed from the measurement site and then readjusted between repetitions to investigate the reproducibility of the measurements.

To determine absolute values for the reflection parameters R and IRC of the saline-cartilage and cartilage-bone interfaces, a rubber disk of known acoustic impedance was used as a reference (calibrator). In the reference measurements, the distance between the ultrasound catheter and the disk was varied from 0.1 to 40.0 mm, using 0.1-mm vertical sampling steps in the direction of the ultrasound beam. In that way, the entire distance range used in the experimental measurements was covered.

6.3 MEASUREMENTS WITH AN ARTHROSCOPIC INDENTATION INSTRUMENT

In study III the experimental data was taken from the study of Kiviranta *et al.* [160] where an arthroscopic hand-held indentation instrument [161] equipped with a miniature unfocused 10-MHz ultrasound transducer (XMS310, diam.=3 mm, Panametrics Inc., Waltham, MA) had been used to measure the ultrasound reflection from the articular surfaces [160]. A hollow external sleeve was attached to the tip of the instrument to keep the distance between the transducer and the cartilage surface constant (3 mm) during the

measurements.

6.4 ULTRASOUND ARTHROSCOPY

The QUI system utilized in the *in vitro* measurements was the same system used for *in vivo* arthroscopies in Kuopio University Hospital (study I) and in Oulu University Hospital (study II). The ultrasound arthroscopies were performed during conventional arthroscopy of knee joints. During the arthroscopies, the antero-lateral and antero-medial portals were used. The ultrasound catheter was inserted into the knee joint through one portal; it was navigated with the help of an arthroscope inserted through the other portal. In addition to imaging, the reflection parameters (R and IRC) and backscattering (AIB) were determined off-line similarly as in *in vitro* procedure.

In study I, the patients (n=2) were referred for arthroscopic examination for surgical repair of an osteochondritis dissecans (OCD) lesion and for evaluation of a surgically repaired anterior cruciate ligament after a sports injury.

In study II, ultrasound images were reconstructed from the raw ultrasound data with custom-made LabVIEW software. In the reconstruction, absolute values of Hilbert transformations, corresponding to each raw signal, were plotted in polar coordinates, and sectors between the values were interpolated. During the arthroscopies (n=11), ultrasound measurements were conducted on each patient at anatomical sites matching the pre-operative CT analysis. All sites were also ICRS graded by means of visual inspection and mechanical probing [94]. The reconstructed ultrasound images were blind coded for the ICRS grading performed by an experienced orthopaedic surgeon not involved in the surgical procedures.

6.5 SCANNING ULTRASOUND SYSTEM

In study I after the measurements with a clinical high frequency intravascular ultrasound device, an UltraPAC scanning ultrasound

system (Physical Acoustics Corporation, Princeton, NJ) was used. The UltraPAC system consists of a 0.5 to 100-MHz ultrasound pulser-receiver board and a 500-MHz 8-bit A/D board. A focused 5-MHz (V307, element diam. = 25.4 mm, confocal beam diam.=600 μm, focal length=49.9 mm, focal zone=8.8 mm, measured bandwidth at -6 dB = 2.7 to 6.3 MHz) or 7.5-MHz ultrasound transducer (V321, element diam.=19.0 mm, confocal beam diam.=600 μm, focal length=50.6 mm, focal zone=8.8 mm, measured bandwidth at -6 dB = 5.2 to 9.7 MHz) was connected to the scanning system in a pulse-echo geometry. For each sample, two measurements were conducted at one local position (single point measurements). In the first measurement, the reflection from articular surface was maximized while in the second measurement, the reflection from cartilage-bone interface was maximized. To achieve this arrangement, samples were manually inclined using two orthogonal goniometers (Edmund Optics Ltd, York, UK) in order to ensure that there was a perpendicular angle of incidence of ultrasound pulse at the investigated interface. The signal gain was adjusted manually to optimize the signal-to-noise ratio for the different interfaces. Data acquisition and control of the ultrasound system were realized with a custom-made LabVIEW (version 6.1, National Instruments, Austin, TX) program. The reference measurements for 5 and 7.5 MHz transducers were conducted with a polished steel plate with a known acoustic impedance.

6.6 MECHANO-ACOUSTIC TESTING DEVICE

In study IV, experimental data was obtained from a previous study [135] where the measurements had been conducted using a custom-made computer-controlled high-resolution mechano-acoustic material testing device [161] equipped with a 500-MHz PAC-AD-500 8-bit AD board and a 0.5- to 100-MHz PAC-IPR-100 pulser-receiver board (Physical Acoustics Corporation, Princeton, NJ). A Panametrics VM-116, contact US transducer (center frequency 10.3 MHz) acted as the compressive platen. The speed of sound in cartilage

was determined after equilibrium preloading (12.5 kPa) using the pulse-echo technique. The time-of-flight was determined as the travel time of the maximum amplitude of the US pulse back and forth through the sample, and the cartilage thickness at preload was determined as the distance between the compressive platens.

6.7 ULTRASOUND PARAMETERS AND ANALYSIS

In studies I and II, the reflection parameters (R and IRC) and AIB [15, 21, 27] were determined with the arthroscopic ultrasound system for cartilage and subchondral bone. For cartilage surface, URI was also determined. URI was calculated from a sector profile consisting of 11 signals (5 points at each side of the point perpendicular to the ultrasound probe). The curvature caused by rotation of the ultrasound probe and the natural contour of the cartilage surface was removed from cartilage surface profiles by using the smoothing spline-fitting technique [16]. In order to ensure normal incidence between the ultrasound pulse and cartilage surface, the ultrasound signal with the smallest time-of-flight (TOF) value was selected for calculation of the reflection parameters (R and IRC) and backscattering AIB.

In study II, the ultrasound parameters of bone (R, IRC and AIB) were corrected with the sample specified reflection at the cartilage surface ($R_{\text{cartilage}}$) and attenuation in cartilage. The attenuation in cartilage was assumed to be constant (α=0.25 Np/mm) [69], and the thickness of the cartilage was determined by assuming a constant ultrasound speed in cartilage (1620 m/s) [69]. Computational corrections for ultrasound reflection and attenuation in overlying cartilage were combined and varied based on values reported in earlier studies [69]. This was done to evaluate the impact of variation in acoustic properties of cartilage on values of ultrasound parameters determined for underlying subchondral bone.

In study III, the experimental raw data from the earlier study [160] were analyzed to calculate the integrated reflection coefficient (IRC) for cartilage. The mixed linear model was used to test the

significance of spatial variation in the *IRC* values separately within the healthy and degenerated cartilage sample groups.

In study IV, experimental ultrasound data for SOS in cartilage was obtained from a previous study [135].

6.8 MECHANICAL TESTING

A custom-made instrument equipped with a high-resolution (0.1 mm) actuator (PM500–1 A, Newport, Irvine, CA, USA) and a load cell (0.005-N resolution) (Sensotec, Columbus, OH, USA) was used in the mechanical measurements of cartilage [157] as a reference in study I. The measurement control and data acquisition were carried out with custom-made software (LabView, National Instruments). For the determination of Young's modulus, a stepwise stress-relaxation protocol in indentation (indenter diam. = 1.04 mm) geometry was used (four steps, 5% strain up to a maximum strain of 20%) [162]. The stress-relaxation test was followed by the measurement of the dynamic modulus (1-Hz sinusoidal loading, 1% strain amplitude) [131]. The values of Young's modulus and dynamic modulus were calculated by assuming cartilage to be a mechanically elastic and isotropic material [163].

6.9 HISTOLOGICAL ANALYSIS

In study I, the integrity of the specimens was evaluated using Mankin scoring [68]. Samples were randomly selected and blind-coded before evaluation. Final Mankin score values were averaged from the results of three independent researchers and rounded to the nearest integer [157].

In studies III and IV, images obtained with a light microscpe were used to construct the geometries for the numerical models. Safranin O stained histological sections (thickness = 3 μm) were prepared from as close as possible to the actual measurement site and imaged using an optical microscope. In study III, the surface profiles of the cartilage samples were obtained from the digitized

histological sections by tracing any abrupt changes in the contrast between the cartilage and the background. In study IV, safranin O stained sections were used to determine the distribution of chondrocytes within cartilage tissue.

6.10 BIOCHEMICAL ANALYSES

The water contents of the samples used in studies I and IV, determined as the difference between the wet weight and dry weight after freeze-drying, were obtained from previous studies [135, 158]. The proteoglycan content used in study IV, measured by determining the content of uronic acid, was from the study of Qu et al. (2007).

6.11 FT-IRIS IMAGING

In studies I and IV PG and collagen distributions were determined from unstained sections (thickness 5 μm) with FT-IRIS (Fourier transform infrared spectroscopy) technique [164, 165]. The collagen content was estimated by integration of the amide I region (1710–1610 cm^{-1}) [164]. In study IV, depth-wise PG and collagen distributions were calculated based on data obtained in a previous study [166].

6.12 MICRO-COMPUTED TOMOGRAPHY IMAGING

In study I, each sample was analysed using micro-scale computed tomography (μCT) imaging (voxel size: 14.93·14.93·14.93 μm^3, tube voltage: 100 kV; SkyScan, Kontich, Belgium) to determine the structure and density of subchondral bone (volume fraction, mineral density, surface-to-volume ratio and trabecular thickness).

6.13 PRE-OPERATIVE CT ARTHROGRAPHY

In study II prior to the CT scan, a 20-mL dose of ioxaglate–gadopentetate contrast agent mixture (105 mM Hexabrix 320, Guerbet, Roissy, France, and 2.5 mM Magnevist, Bayer HealthCare Pharmaceuticals, Berlin, Germany; diluted in 0.9% saline) was injected intra-articularly. After the injection, the patient performed active flexion–extension of the knee for 5 min to facilitate that there was an even distribution of the contrast agent in the joint space. After this exercise period, the knee joint of the patient was scanned using a clinical 64-slice CT scanner (Discovery PET/CT 690, GE Medical Systems, Waukesha, WI, USA) with a tube voltage of 100 kV, tube current of 160 mA and current time product 146 mAs. The focal spot diameter and pitch were 0.7 mm and 0.53, respectively. From the arthrographic CT images, the thickness of the subchondral plate and X-ray attenuation (HU) in subchondral bone were determined for each patient at seven anatomical locations - lateral trochlea, medial trochlea, lateral femoral condyle, medial femoral condyle, lateral tibial condyle, medial tibial condyle and central patella, corresponding to the sites defined in the ICRS evaluation system. The 3D Slicer (www.slicer.org) software was used for 3D image analysis of subchondral bone [167].

The parameters used in the studies are summarized in Table 6.2.

6.14 FDTD MODELING

In studies III and IV, a sample-specific FDTD models for ultrasonic measurements of articular cartilage in pulse-echo geometry were developed. In study III, the FDTD model for ultrasound reflection from the cartilage surface was constructed using Wave 2000 Plus 3.00 R3 software (CyberLogic Inc., New York, NY, USA). In study IV, Wave 3000 Plus 4.20 R1 software (CyberLogic Inc., New York, NY, USA) was used to simulate the SOS in cartilage. Wave 3000 Plus was used for 2D simulations by limiting the grid in the y-direction with longitudinal boundary conditions. Both softwares can solve an

Table 6.2: Summary of parameters compared in studies I-IV.

Study and methods	**Parameters (unit or range)**
Study I	
Ultrasound	R (%), IRC (dB), AIB (dB), URI (μm), Cartilage thickness (mm)
Mechanical testing	E (MPa)
Biochemical analysis	Water content (%), Uronic acid content (%)
Histological analysis	Mankin score (range: 0-14)
μCT imaging	Cartilage thickness (mm)
Study II	
Ultrasound	R (%), IRC (dB), AIB (dB), URI (μm) Cartilage thickness (mm)
Conventional arthroscopy	ICRS-grade (range: 0-4)
Preoperative CT	Plate thickness (μm), X-ray attenuation (HU)
Study III	
Ultrasound	R (%), IRC (dB), URI (μm)
Material parameters	E (MPa), λ (MPa), μ (MPa), ν, ρ (kg/m^3), v_l (m/s), v_t (m/s)
Model output	R (%), IRC (dB), URI (μm)
Study IV	
Ultrasound	SOS (m/s)
Material parameters	E (MPa), λ (MPa), μ (MPa), ν, ρ (kg/m^3), v_l (m/s), v_t (m/s)
Model output	SOS (m/s)

acoustic wave equation within each homogenous grid element and compute the displacement vector at each time step of the simulation based on the equation (4.7). The input signal waveforms of the transducers were digitized from the datasheets of the transducers used in the corresponding experimental measurements.

In study III, the model geometry was identical with the experimental geometry containing a single-phasic homogeneous material (cartilage) immersed in water. The surface roughness profiles of

the samples, obtained from the digitized histological sections, were implemented in the model individually for each sample. Three different sets of simulations were made (Table 6.3): 1) To evaluate systematically the effect of the roughness of the cartilage surface on the integrated reflection coefficient (IRC), seven artificial roughness profiles (roughness = $0.0 \ldots 29.7$ μm) were generated with Matlab v.7.6.0 (MathWorks Inc., Natick, MA) using a custom-made algorithm. 2) The effect of the ultrasound angle of incidence was studied with three combinations of values of material parameters (ρ, λ and μ). The above-mentioned seven artificial roughness profiles were inclined in steps of 1° from -5° to 5°, with the 0° corresponding to the normal incidence of the ultrasound pulse. IRC was calculated for all simulations. 3) In order to investigate the effect of integrity of the cartilage surface, one representative digitized histological human cartilage section per sample was selected after visually evaluating all sections prepared from each sample. The section was implemented into the model to simulate the reflection of the ultrasound from the cartilage surfaces with visually intact appearance and with different grades of surface degeneration. The viscous damping parameters for cartilage were set to constant values $\eta = 1.75$ N $\cdot$ s/m^2 (shear viscosity) and $\phi = 199.7 \times 10^{-6}$ N $\cdot$ s/m^2 (bulk viscosity).

Table 6.3: Summary of material parameters used in studies III and IV.

Study / material	ρ (kg/m^3)	λ (MPa)	μ (MPa)
III			
Cartilage	$1010 - 1100$	$2342.7 - 3306.9$	$3.3 - 33.4$
IV			
Water	1000	2241	0
Chondrocytes	1580	3410	0
PGs	1350	4120	0.017
Collagen	1350	7487	0.017
Steel	8030	100868	78170

In study IV, sample specific simulation geometries (n=28), equivalent to the experimental setup [135], were created based on histological sections with custom-made software in Matlab 2012a (MathWorks Inc., Natick, MA). The cartilage matrix was assumed to consist of chondrocytes, water and solid matrix (PG and collagen). First, chondrocytes were implemented based on microscopic images of safranin O stained sections. The extracellular matrix was divided into 40 depth-wise layers. The water content was implemented based on biochemical analyses. The rest of the extracellular space was assumed to be solid containing PG and collagen. PG and collagen distributions were determined with the FT-IRIS technique and implemented as a solid matrix containing 1:3 PG and 2:3 collagen [168]. Depth-wise water content was then calculated. The elastic parameters for PG and collagen were calculated based on their acoustical properties as reported in the literature [129,169]. In each layer the elastic parameters of the FDTD grid were calculated as the weighted average of all components (PG, collagen and water). Finally, SOS in each sample was determined based on the simulated data. A summary of the model parameters is provided in Table 6.3.

By using one sample with original a simulated SOS value of 1676 m/s the effects of PGs and collagen contents were studied with simulations in which collagen or PGs were completely removed, leaving other model features untouched. The sensitivity of simulated SOS for changes in material parameter values ρ, λ and μ was investigated by varying each parameter individually (change of -10%, -5%, 5% or 10%).

6.15 STATISTICAL METHODS

Statistical analyses were conducted with SPSS software (IBM SPSS Statistics for Windows, Version 19.0. Armonk, IBM Corp., NY, USA). In studies II and IV, the Wilcoxon signed ranks, Kruskal-Wallis and Mann–Whitney tests were used to compare averages. The different scoring methods were compared with the inter-item

correlation analysis.

7 Results

7.1 ULTRASOUND MEASUREMENTS *IN VITRO*

The mean values of the ultrasound parameters measured in study I are presented in Table 7.1. Significant linear correlations were found between the reflection coefficients (R, IRC) of cartilage surface and the Mankin score or Young's modulus ($|r| > 0.56$, $p < 0.05$) (Table 7.2). The linear correlations between the apparent integrated backscattering (AIB) or ultrasound roughness index (URI) and the mechanical or structural parameters of cartilage did not achieve statistical significance ($p > 0.05$). Further, there were no significant correlations between the ultrasound parameters and the collagen content determined with FT-IRIS.

All the bone ultrasound parameters (R, IRC, AIB) correlated significantly with the bone surface/volume-ratio ($|r| > 0.70$, $p < 0.05$) and trabecular thickness ($|r| > 0.59$, $p < 0.05$, (7.2). Furthermore, a significant correlation was detected between R and bone mineral density ($r = 0.65$, $p < 0.05$). The measurements of reflection and backscatter parameters (R, IRC, AIB) for articular cartilage and subchondral bone tissue were highly reproducible ($sCV(\%) = 0.4 - 3.0$), whereas the reproducibility of the ultrasound roughness index (URI) was weaker (17.0%).

The cartilage-subchondral bone interface was visible in all of the ultrasound measurements, which made it possible to evaluate the thickness of the cartilage. A significant linear correlation was found between the cartilage thickness determined with ultrasound and μCT-imaging ($r = 0.75$, $p < 0.01$).

There were significant correlations between the 5 MHz ultrasound reflection coefficients (R, IRC) and the collagen content determined with FT-IRIS ($r > 0.57$, $p < 0.05$). However, there were no significant linear correlations between the ultrasound parameters (R, IRC, AIB and URI) and the mechanical and structural parameters of cartilage (Table 7.2). All the bone ultrasound parameters (R,

IRC, *AIB*) determined with both the frequencies (5 MHz and 7.5 MHz) correlated significantly with the bone surface/volume-ratio ($|r| > 0.59$, $p < 0.05$). In addition, at both frequencies the *AIB* and the trabecular thickness were significantly correlated ($|r| > 0.58$, $p < 0.05$). Furthermore, at 5 MHz the reflection coefficient of cartilage-bone interface was significantly correlated with the trabecular thickness ($r = 0.69$, $p < 0.01$, Table 7.2).

There was consistency between the ultrasound reflection parameters of the cartilage-bone interface obtained with the laboratory system and those estimated with the clinical device. All the reflection coefficients (*R*, *IRC*) determined with different instruments were significantly correlated ($r > 0.73$, $p < 0.01$).

A significant correlation ($r = -0.52$, $p < 0.01$) between simulated *IRC* and the roughness of the human samples was found in study III.

Table 7.1: Values (mean±SD) of reflection parameters (R and IRC), apparent integrated backscattering coefficient (AIB) and ultrasound roughness index (URI) determined with ultrasound in vitro.

Cartilage		Bone	
Parameter	**Value**	**Parameter**	**Value**
9 MHz arthroscopic ultrasound system			
R_c (%)	6.7 ± 2.5	R_b (%)	23.4 ± 10.1
IRC_c (dB)	-23.8 ± 4.1	IRC_b (dB)	-21.9 ± 4.8
AIB_c (dB)	-45.5 ± 4.0	AIB_b (dB)	-43.9 ± 5.5
URI_c (μm)	13.9 ± 5.2		
5 MHz scanning ultrasound system			
R_c (%)	6.5 ± 1.6	R_b (%)	40.1 ± 17.1
IRC_c (dB)	-24.1 ± 2.0	IRC_b (dB)	-9.0 ± 3.6
AIB_c (dB)	-50.7 ± 4.2	AIB_b (dB)	-15.5 ± 5.2
7.5 MHz scanning ultrasound system			
R_c (%)	6.5 ± 2.9	R_b (%)	38.6 ± 21.7
IRC_c (dB)	-25.3 ± 6.4	IRC_b (dB)	-15.8 ± 5.9
AIB_c (dB)	-53.2 ± 4.0	AIB_b (dB)	-27.9 ± 11.6

Table 7.2: Spearman's correlation coefficients between ultrasound parameters (R, IRC, AIB and URI) and tissue characteristics. The reflection coefficients of bone surface (R, IRC) were significantly related to surface/volume ratio.

	Mankin score	**Young's modulus**	**Water content**	**Uronic acid**
Cartilage				
9 MHz arthroscopic ultrasound system				
R_c	-0.61*	0.57*	-0.37	0.52
IRC_c	-0.64*	0.56*	-0.37	0.50
AIB_c	-0.09	-0.26	-0.51	-0.22
URI_c	0.43	-0.18	0.18	-0.13
5 MHz scanning ultrasound system				
R_c	-0.41	0.50	-0.49	0.29
IRC_c	-0.41	0.55	-0.42	0.35
AIB_c	-0.11	0.19	-0.22	0.46
7.5 MHz scanning ultrasound system				
R_c	-0.11	0.25	-0.21	0.27
IRC_c	-0.20	0.35	-0.31	0.40
AIB_c	0.14	0.54	-0.03	0.38
	Volume fraction	**Young's modulus**	**Surface/volume ratio**	**Trabecular thickness**
Bone				
9 MHz arthroscopic ultrasound system				
R_b	0.36	0.65*	-0.88**	0.82**
IRC_b	0.07	0.48	-0.82**	0.72**
AIB_b	-0.01	0.41	-0.70*	0.59*
5 MHz scanning ultrasound system				
R_b	0.34	0.31	-0.74**	0.69**
IRC_b	0.01	0.26	-0.59*	0.41
AIB_b	0.35	0.39	-0.78**	0.72**
7.5 MHz scanning ultrasound system				
R_b	0.18	0.29	-0.61*	0.48
IRC_b	0.10	0.39	-0.62*	0.45
AIB_b	0.31	0.42	-0.68*	0.58*

*$p < 0.05$
**$p < 0.01$

7.2 ULTRASOUND ARTHROSCOPIES *IN VIVO*

In studies I and II, all of the ultrasound arthroscopies were successful, enabling evaluation of articular cartilage, subchondral bone and

meniscus. In addition, they made it possible to achieve simultaneous imaging of articular cartilage and subchondral bone. This enabled the evaluation of cartilage thickness. In the OCD case (study I), the lesion site was detected and its dimensions could be measured with ultrasound. Furthermore, the success of the repair operation could be evaluated with ultrasound imaging. In study II, ultrasound imaging of a particular anatomical location could not be performed in 7 out of 77 examined regions because of the non-optimal maneuverability and fragility of the ultrasound catheter.

The ICRS grades determined during conventional arthroscopy and ultrasound arthroscopy differed (Table 7.4). The median values of grades based on ultrasound images were equal to or greater than those based on conventional arthroscopic evaluation at all anatomical locations (Figure 7.1). On the basis of the inter-item correlation analysis, there was a relatively poor agreement between the ICRS grades determined by conventional arthroscopy and those with ultrasound arthroscopy was relatively poor ($r = 0.57$).

Reflection (R and IRC) and backscattering (AIB) values (Table 7.3) determined for cartilage were significantly ($p < 0.05$) lower in group 2 (ICRS grade 2) than in groups 0 and 1 (ICRS grades 0 and 1). No significant differences were observed in ultrasound parameters of subchondral bone between the sample groups with different ICRS grades. Furthermore, there were no significant correlations between the ultrasound parameters and subchondral plate thickness or X-ray attenuation in subchondral bone.

Computational corrections After different corrections for bone parameters (R, IRC and AIB) significant correlations were detected ($r > 0.73$, $p < 0.01$) between uncorrected and corrected values. On the basis of numerical simulations, the effect attenuation in cartilage was found to be greater than the effect of reflection at the articular surface on values of ultrasound reflection at the cartilage–bone interface (Figure 7.2).

Table 7.3: Values (mean±SD) of ultrasound reflection parameters (R and IRC), apparent integrated backscattering coefficient (AIB) and ultrasound roughness index (URI) determined with the arthroscopic ultrasound system in vivo as a function of ICRS grade. Reflection and backscattering values determined for cartilage were significantly ($p < 0.05$) lower in group 2 (ICRS grade 2) than in groups 0 and 1 (ICRS grades 0 and 1).

Ultrasound parameters	**Grade 0**	**1**	**2**
Cartilage			
R_c (%)	3.5±2.3	2.5±1.2	1.2±0.5
IRC_c (dB)	-30.7±5.9	-32.9±4.0	−38.7±3.3
AIB_c (dB)	-44.7±8.1	-46.8±5.8	−52.0±6.7
URI_c (μm)	11.5±9.0	14.6±11.2	18.2±9.8
Bone			
R_b (%)	13.9±7.1	15.3±7.5	15.9±6.7
IRC_b (dB)	-26.7±6.5	-26.6±7.8	−23.9±5.5
AIB_b (dB)	-42.0±3.8	-42.3±7.9	−40.3±5.0

Table 7.4: Comparison between ICRS grades obtained by conventional and ultrasound arthroscopies. Ultrasound arthroscopy resulted higher scores than conventional arthroscopy.

ICRS grade	**Conventional arthroscopy**	**Ultrasound arthroscopy**
0, normal	24	13
1, nearly normal	21	23
2, abnormal	22	14
3, severely abnormal	3	9
4, severely abnormal	0	3

7.3 FDTD MODELING

When the roughness of the surface of the cartilage was increased in the model from 0 μm to 30 μm, the change in the values of the *IRC* was -8 to -14 dB for any chosen combination of values of the material parameters. In addition, a threshold was found between the roughness values from 7.8 μm to 13.1 μm, beyond which, when

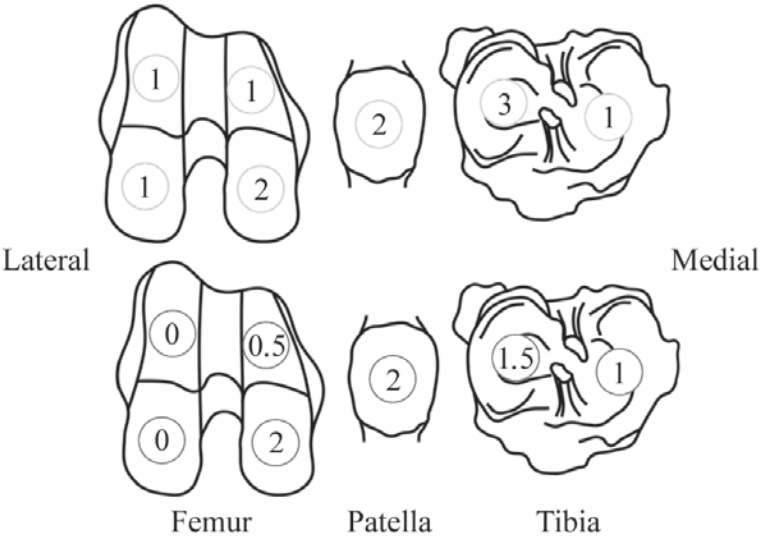

Figure 7.1: Comparison (median values) of ICRS grades determined with ultrasound arthroscopy (above) and conventional arthroscopy (bellow).

the roughness increased, the reflection of the ultrasound at the normal angle of incidence diminished and the angular dependence of the reflection disappeared. The numerically evaluated IRC values for the same samples correlated significantly with the roughness ($r = -0.52$, $p < 0.01$). However, there was no significant correlation between the experimentally and numerically determined values of the IRC.

In study IV, a significant linear correlation was revealed between the experimental and simulated SOS values ($r = 0.82$, $p < 0.05$) (Figure 7.3). The simulated SOS values were systematically higher (100 m/s average difference) ($p < 0.05$). Total removal of PG and collagen reduced SOS values from 1676 m/s to 1660 m/s and 1518 m/s, respectively. Changes in the values of the material parameters (ρ, λ and μ) from -10% to 10% produced -26...25 m/s changes in SOS (Table 7.5).

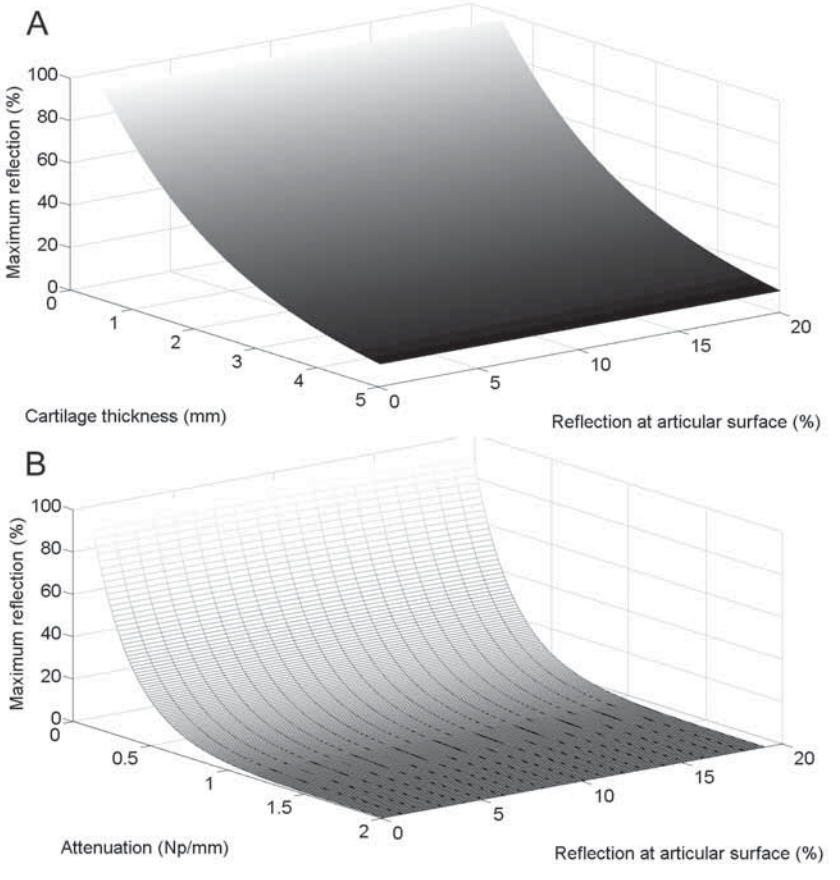

Figure 7.2: A) Ultrasound attenuation (α=0.25 Np/mm) in cartilage plays a major role when ultrasound parameters of bone (e.g. reflection at cartilage-bone interface, y-axis in the figures) are corrected with reflection and attenuation in cartilage. B) The attenuation (0.1 . . . 2 Np/mm) has a major role also when cartilage thickness is constant (2.0 mm).

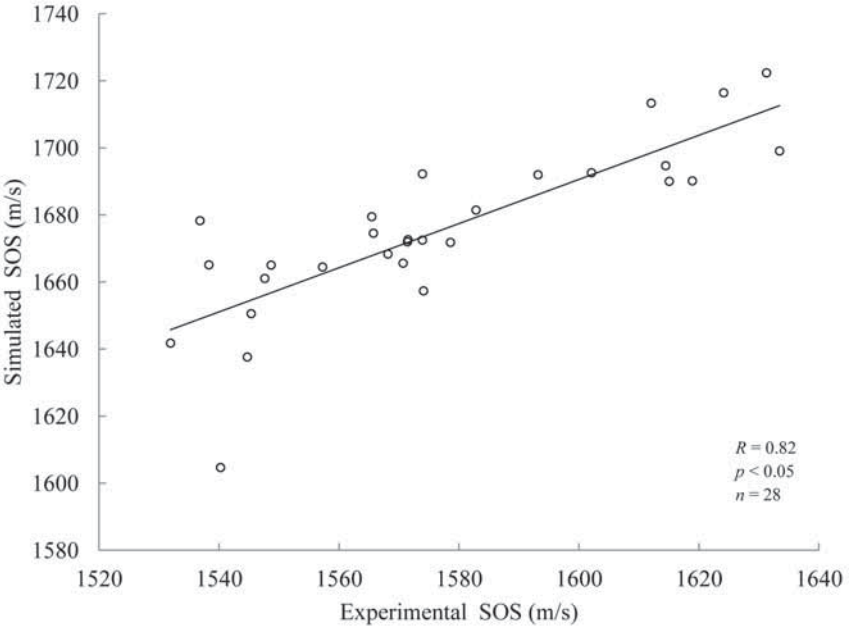

Figure 7.3: Experimental and simulated SOS values. Despite the relatively strong correlation the simulated SOS values were systematically higher than those determined experimentally (100 m/s average difference). Simulated SOS = 0.66 × experimental SOS + 636 m/s.

Table 7.5: SOS (m/s) in cartilage as a function of changes in each material parameter. The parameters were varied one by one, leaving the other model features unchanged.

	PG			Collagen		
Change (%)	ρ	λ	μ	ρ	λ	μ
-10	1682	1669	1676	1689	1650	1676
-5	1679	1672	1676	1682	1663	1676
0	1676	1676	1676	1676	1676	1676
5	1673	1679	1676	1669	1688	1676
10	1669	1683	1676	1663	1701	1676

8 Discussion

The first aim of this thesis was to evaluate the potential of an arthroscopic ultrasound technique for conducting a simultaneous assessment of articular cartilage and subchondral bone *in vitro* and *in vivo*. In study I, the feasibility of the technique was investigated with human osteochondral samples and two clinical arthroscopies. A series of arthroscopies was conducted in study II in order to study the additional value of arthroscopic ultrasound imaging when evaluating the scoring of cartilage injuries and tissue integrity. The second aim was to deepen the understanding of the interplay between ultrasound and cartilage properties to improve interpretation of experimental ultrasound data by developing specific FDTD-models for ultrasound propagation in cartilage.

8.1 SIMULTANEOUS ULTRASOUND ASSESSMENT OF ARTICULAR CARTILAGE AND SUBCHONDRAL BONE

The correlations between the ultrasound reflection parameters (R and IRC) determined with the arthroscopic ultrasound system and the reference parameters (Mankin score, Young's modulus, water content and uronic acid content) are consistent with those reported in previous studies with the laboratory ultrasound instrumentation in use [16, 170]. The failure to detect an association between AIB and the structural and mechanical parameters of cartilage may be due the fact that only minor degenerative changes were present in the studied cartilage samples. In early-stage OA, the alterations are limited to the surface of cartilage, and changes in ultrasound scattering may not occur within the deeper layers of cartilage.

Ultrasound measurements through articular cartilage were found to be moderately sensitive to degenerative changes in subchondral bone. The backscattering (AIB) in subchondral bone tissue was significantly related to surface/volume ratio and trabecular thickness.

In addition, there were significant correlations between reflection coefficients (R and IRC) of the cartilage-bone interface and surface/volume ratio and trabecular thickness of subchondral bone. The peri-articular bone tends to change early in the development of OA. These changes include an increase in the subchondral bone thickness, a decrease in subchondral trabecular bone mass and advancement of the zone of calcified cartilage [171]. Although there may be no direct causal relationship between the trabecular thickness and ultrasound reflection coefficient of the cartilage-bone interface, an increase in trabecular thickness is often related to thickening of the subchondral plate and an increase in its degree of mineralization [171]. This may explain the observed correlations between the reflection coefficients (R and IRC) and trabecular thickness. The present findings support the feasibility of using the arthroscopic ultrasound technique in OA diagnosis and are in line with the previous studies favouring the use of quantitative ultrasound for diagnosis of degenerative changes in bone [172–174].

In the present study, cartilage thickness could be measured with an arthroscopic 9 MHz ultrasound probe. However, the correlation between the thickness values determined with μCT and ultrasound ($r = 0.75$, $p < 0.01$) was not as high as reported earlier [18]. This is probably due to the difference in the applied ultrasound frequencies (9 MHz vs. 22 MHz). The lower frequency applied in the present study limits the axial resolution resulting in ans inaccuracy in determining the thickness values. Moreover, the determination of cartilage thickness requires an assumption of constant ultrasound speed in the cartilage. The sound speed depends on the degenerative state of cartilage tissue [135], limiting the technique's reliability for determination of cartilage thickness.

The lack of significant correlations between the ultrasound parameters determined with the scanning ultrasound system and the mechanical and structural parameters of cartilage may be explained by use of low frequencies (5-7.5 MHz vs. 9 MHz). In addition, the transducers differ in sizes, energies and waveforms. However, the correlations between the ultrasound parameters of bone and the

μCT parameters that describe bone structure and density were consistent with those obtained with the arthroscopic ultrasound device. This was expected since frequencies of 5-10 MHz have been successfully used in ultrasound studies of bone [175, 176]. The differences in the correlations for cartilage and cartilage-bone interfaces, as measured with the applied ultrasound frequencies, may be related to the mechanical and structural properties of cartilage and bone. In cartilage, the main scatterers are the collagen network and chondrocytes (diam. < 20 μm) [177] whereas in bone, scattering is mainly caused by trabecular structures (diam. > 100 μm [178].

ICRS grades obtained with ultrasound arthroscopy were higher than those obtained with conventional arthroscopy. Furthermore, the inter-item correlation analysis revealed that there was poor agreement between the grades derived from conventional and ultrasound arthroscopy. This was expected, as ultrasound visualizes both cartilage and subchondral bone, revealing additional information on cartilage degeneration, for example, the relative depth of the lesion. Based on the present results, the estimated lesion depth is systematically too shallow when assessed with conventional arthroscopy. To avoid this problem, orthopaedic surgeons should be aware of the limitations of conventional arthroscopy with its inherent risk of underestimating chondral injuries.

Potentially, ultrasound arthroscopy may be considered as a quantitative tool to improve the poor reproducibility of conventional arthroscopy-based ICRS grading as reported by others [12]. However, the reproducibility of ultrasound arthroscopy-based ICRS scoring is still unknown and this will demand further research.

In the present study, no significant correlations were found between bone ultrasound (9 MHz) parameters and subchondral plate thickness or X-ray attenuation in subchondral trabecular bone, as determined with pre-operative CT-arthrography. Issues related to the resolution of CT arthrography and limitations related to the performance of the arthroscopic ultrasound probe used in the present study may partially explain this unexpected result. In order to overcome the challenges related to the complexity of *in vivo* mea-

surement, insufficient maneuverability and transmit power of the applied ultrasound probe, an arthroscopic ultrasound probe with optimal catheter and transducer geometries and optimal waveform and frequency of the transmitted pulse needs to be designed.

As attenuation in cartilage was found to be the dominant factor affecting the quantitativeness of ultrasound measurement of bone in study II, implementation of attenuation correction should be further developed; whereas reflection from the cartilage surface might be even ignored.

8.2 FDTD MODEL OF ULTRASOUND PROPAGATION IN ARTICULAR CARTILAGE

In study III, the change in the IRC values between the smooth (roughness = 0 μm) and rough (roughness = 30 μm) cartilage was roughly -8 to -14 dB, regardless of the material parameters. However, the lack of correlation ($r = 0.16$) between the experimental and the modeled IRC values, indicates that the material parameters also contribute significantly to the value of the IRC .

When the roughness of the cartilage surface was increased, the angular dependence of the reflection (IRC) disappeared. This agrees with previous experimental work pointing to the existence of such a boundary value between roughnesses 4.8 and 26.9 μm [179]. This suggests that if the angle of incidence of the ultrasound beam is not carefully controlled in the measurements, the reliability of the ultrasound diagnosis of the earliest OA changes in articular surface might be compromised. With a phased array transducer, this problem could be solved by adjusting the transducer in a position which TOFs measured with individual transducers are similar.

In study IV, the simulated and experimental SOS values were linearly correlated. This suggests that composition and mechanical properties of the samples had been successfully implemented in the model. Previous experimental studies have shown that cartilage composition [129] and mechanical properties [180] are significantly related to SOS. Thus, a feasible numerical model must include suffi-

cient information on the composition and the mechanical properties of cartilage and be able to predict SOS based on this information.

The present model produced systematically greater SOS values than the experimentally-derived values. In the model, SOS is directly affected by the selection of material parameters of tissue constituents. In the present, study the values of material parameters were calculated using the information from the literature as a volume-weighted average. However, values of density and Lamé parameters for each component (water, PG, collagen and chondrocyte) present in articular cartilage have not been comprehensively reported in the literature. In the future, the input parameters of the model could be optimized by fitting the model to the experimental data.

Based on the simulations where the values of the material parameters were varied density of the solid matrix should be higher or values of the first Lamé parameters should be lower to achieve a closer agreement with experimentally determined sound speed values. Removal of collagen caused a major change in SOS (from 1676 to 1518 m/s), implying a significant role of collagen.

Cartilage is a poroviscoelastic, inhomogeneous and anisotropic material with a complicated composition and structure. In the current model, articular cartilage was significantly simplified: many characteristics such as the viscous attenuation and its detailed structure (*e.g.* collagen fibril network) were omitted. Implementation of viscous attenuation would have required knowledge of bulk and shear viscosities for each constituent.

In articular cartilage, simultaneous changes in composition (water, PG and collagen contents) and the structure of a solid matrix affect its acoustical properties in a complex manner. Thus, only modeling could provide feasible means to investigate the effects of individual constituents on SOS. The present simplified model could only provide reliable SOS data. If one wishes to determine more complicated ultrasound parameters (reflection, attenuation, backscattering) then more detailed and complex models will be needed.

9 Conclusions

In this thesis, the feasibility of using 5-9 MHz ultrasound assessment for simultaneous measurements of articular cartilage and subchondral bone was investigated. Furthermore, the value of the additional information provided by ultrasound arthroscopy on ICRS grading was assessed. With numerical models, ultrasound reflection was investigated from varying surface roughness, material parameters (Young's modulus, density, longitudinal, and transversal velocities) and inclination of the samples. Finally, a sample specific anisotropic FDTD model of articular cartilage containing chondrocytes, proteoglycans, collagen and water was devised and evaluated.

Based on the studies included in this thesis, the following conclusions may be drawn:

- Degenerative changes of articular cartilage and subchondral bone may be detected with ultrasound arthroscopy.
- In order to harness the full potential of ultrasound arthroscopy, an arthroscopic ultrasound probe with optimal catheter and transducer geometries and an improved waveform and frequency of the transmitted pulse needs to be designed.
- The FDTD method is a feasible way to model the effects of varying surface roughness, cartilage constituents and ultrasound angle of incidence on the ultrasound reflection and propagation.
- The numerical approach model helps to understand the roles of cartilage constituents in ultrasound propagation.

Bibliography

[1] A. Benninghoff, "Form und Bau der Gelenkknorpel in ihren Beziehungen zur Funktion.," *Zeitschrift ür Zellforschung und Mikroskopische Anatomie* **2,** 783–862 (1925).

[2] V. C. Mow, M. H. Holmes, and W. M. Lai, "Fluid transport and mechanical properties of articular cartilage: a review.," *Journal of biomechanics* **17,** 377–94 (1984).

[3] A. Maroudas, M. T. Bayliss, and M. F. Venn, "Further studies on the composition of human femoral head cartilage.," *Annals of the rheumatic diseases* **39,** 514–23 (1980).

[4] E. M. Hasler, W. Herzog, J. Z. Wu, W. Müller, and U. Wyss, "Articular cartilage biomechanics: theoretical models, material properties, and biosynthetic response.," *Critical reviews in biomedical engineering* **27,** 415–88 (1999).

[5] J. P. Arokoski, J. S. Jurvelin, U. Väätäinen, and H. J. Helminen, "Normal and pathological adaptations of articular cartilage to joint loading.," *Scandinavian journal of medicine & science in sports* **10,** 186–98 (2000).

[6] J. A. Buckwalter and H. J. Mankin, "Instructional Course Lectures, The American Academy of Orthopaedic Surgeons - Articular Cartilage. Part I: Tissue Design and Chondrocyte-Matrix Interactions.*†," *The Journal of Bone & Joint Surgery* **79,** 600–11 (1997).

[7] J. A. Buckwalter and J. Martin, "Degenerative joint disease.," *Clinical symposia (Summit, N.J. : 1957)* **47,** 1–32 (1995).

[8] N. Arden and M. C. Nevitt, "Osteoarthritis: epidemiology.," *Best practice & research. Clinical rheumatology* **20,** 3–25 (2006).

[9] M. Heliövaara, P. Slätis, and P. Paavolainen, "Nivelrikon esiintyvyys ja kustannukset.," *Duodecim* 1869–1874 (2008).

[10] W. P. Chan, P. Lang, M. P. Stevens, K. Sack, S. Majumdar, D. W. Stoller, C. Basch, and H. K. Genant, "Osteoarthritis of the knee: comparison of radiography, CT, and MR imaging to assess extent and severity.," *AJR. American journal of roentgenology* **157,** 799–806 (1991).

[11] X. Li and S. Majumdar, "Quantitative MRI of articular cartilage and its clinical applications.," *Journal of magnetic resonance imaging : JMRI* **38,** 991–1008 (2013).

[12] G. Spahn, H. M. Klinger, M. Baums, U. Pinkepank, and G. O. Hofmann, "Reliability in arthroscopic grading of cartilage lesions: results of a prospective blinded study for evaluation of inter-observer reliability.," *Archives of orthopaedic and trauma surgery* **131,** 377–81 (2011).

[13] G. Spahn, H. M. Klinger, and G. O. Hofmann, "How valid is the arthroscopic diagnosis of cartilage lesions? Results of an opinion survey among highly experienced arthroscopic surgeons.," *Archives of orthopaedic and trauma surgery* **129,** 1117–21 (2009).

[14] R. S. Adler, D. K. Dedrick, T. J. Laing, E. H. Chiang, C. R. Meyer, P. H. Bland, and J. M. Rubin, "Quantitative assessment of cartilage surface roughness in osteoarthritis using high frequency ultrasound.," *Ultrasound in Medicine & Biology* **18,** 51–58 (1992).

[15] S. Saarakkala, J. Töyräs, J. Hirvonen, M. S. Laasanen, R. Lappalainen, and J. S. Jurvelin, "Ultrasonic quantitation of superficial degradation of articular cartilage.," *Ultrasound in medicine & biology* **30,** 783–92 (2004).

[16] S. Saarakkala, M. S. Laasanen, J. S. Jurvelin, and J. Töyräs, "Quantitative ultrasound imaging detects degen-

erative changes in articular cartilage surface and subchondral bone.," *Physics in medicine and biology* **51,** 5333–46 (2006).

[17] E. Chérin, A. Saïed, B. Pellaumail, D. Loeuille, P. Laugier, P. Gillet, P. Netter, and G. Berger, "Assessment of rat articular cartilage maturation using 50-MHz quantitative ultrasonography.," *Osteoarthritis and cartilage* **9,** 178–86 (2001).

[18] J. Töyräs, J. Rieppo, M. T. Nieminen, H. J. Helminen, and J. S. Jurvelin, "Characterization of enzymatically induced degradation of articular cartilage using high frequency ultrasound.," *Physics in Medicine and Biology* **44,** 2723–2733 (1999).

[19] H. J. Nieminen, J. Töyräs, J. Rieppo, M. T. Nieminen, J. Hirvonen, R. Korhonen, and J. S. Jurvelin, "Real-time ultrasound analysis of articular cartilage degradation in vitro.," *Ultrasound in medicine & biology* **28,** 519–25 (2002).

[20] M. Laasanen, J. Töyräs, A. Vasara, S. Saarakkala, M. Hyttinen, I. Kiviranta, and J. S. Jurvelin, "Quantitative ultrasound imaging of spontaneous repair of porcine cartilage.," *Osteoarthritis and Cartilage* **14,** 258–263 (2006).

[21] T. Virén, S. Saarakkala, J. S. Jurvelin, H. J. Pulkkinen, V. Tiitu, P. Valonen, I. Kiviranta, M. J. Lammi, and J. Töyräs, "Quantitative evaluation of spontaneously and surgically repaired rabbit articular cartilage using intra-articular ultrasound method in situ.," *Ultrasound in medicine & biology* **36,** 833–9 (2010).

[22] S. L. Myers, K. Dines, D. A. Brandt, K. D. Brandt, and M. E. Albrecht, "Experimental assessment by high frequency ultrasound of articular cartilage thickness and osteoarthritic changes.," *The Journal of rheumatology* **22,** 109–16 (1995).

[23] S. Saarakkala, S.-Z. Wang, Y.-P. Huang, J. S. Jurvelin, and Y.-P. Zheng, "Characterization of center frequency and bandwidth of broadband ultrasound reflected by the articular cartilage to

subchondral bone interface.," *Ultrasound in medicine & biology* **37,** 112–21 (2011).

[24] A. Saïed, E. Chérin, H. Gaucher, P. Laugier, P. Gillet, J. Floquet, P. Netter, and G. Berger, "Assessment of articular cartilage and subchondral bone: subtle and progressive changes in experimental osteoarthritis using 50 MHz echography in vitro.," *Journal of bone and mineral research* **12,** 1378–86 (1997).

[25] S. E. Nissen and P. Yock, "Intravascular ultrasound: novel pathophysiological insights and current clinical applications.," *Circulation* **103,** 604–16 (2001).

[26] E. Kaleva, T. Viren, S. Saarakkala, J. Sahlman, J. Sirola, J. Puhakka, T. Paatela, H. Kroger, I. Kiviranta, J. S. Jurvelin, and J. Töyräs, "Arthroscopic Ultrasound Assessment of Articular Cartilage in the Human Knee Joint: A Potential Diagnostic Method.," *Cartilage* **2,** 246–253 (2010).

[27] T. Virén, S. Saarakkala, E. Kaleva, H. J. Nieminen, J. S. Jurvelin, and J. Töyräs, "Minimally invasive ultrasound method for intra-articular diagnostics of cartilage degeneration.," *Ultrasound in medicine & biology* **35,** 1546–54 (2009).

[28] B. E. Treeby, J. Jaros, A. P. Rendell, and B. T. Cox, "Modeling nonlinear ultrasound propagation in heterogeneous media with power law absorption using a k-space pseudospectral method.," *The Journal of the Acoustical Society of America* **131,** 4324–36 (2012).

[29] U. Vyas and D. Christensen, "Ultrasound beam simulations in inhomogeneous tissue geometries using the hybrid angular spectrum method.," *IEEE transactions on ultrasonics, ferroelectrics, and frequency control* **59,** 1093–100 (2012).

[30] E. Bossy, F. Padilla, F. Peyrin, and P. Laugier, "Three-dimensional simulation of ultrasound propagation through trabecular bone structures measured by synchrotron microtomography.," *Physics in medicine and biology* **50,** 5545–56 (2005).

[31] F. Padilla, E. Bossy, G. Haiat, F. Jenson, and P. Laugier, "Numerical simulation of wave propagation in cancellous bone.," *Ultrasonics* **44 Suppl 1,** e239–43 (2006).

[32] J. Kaufman, G. Luo, and R. Siffert, "Ultrasound simulation in bone.," *Ultrasonics, Ferroelectrics and . . .* **55** (2008).

[33] V. Le Floch, D. J. McMahon, G. Luo, A. Cohen, J. J. Kaufman, E. Shane, and R. S. Siffert, "Ultrasound simulation in the distal radius using clinical high-resolution peripheral-CT images.," *Ultrasound in medicine & biology* **34,** 1317–26 (2008).

[34] C. B. Machado, W. C. D. a. Pereira, M. Granke, M. Talmant, F. Padilla, and P. Laugier, "Experimental and simulation results on the effect of cortical bone mineralization in ultrasound axial transmission measurements: a model for fracture healing ultrasound monitoring.," *Bone* **48,** 1202–9 (2011).

[35] V. C. Mow, A. Ratcliffe, and A. R. Poole, "Cartilage and diarthrodial joints as paradigms for hierarchical materials and structures.," *Biomaterials* **13,** 67–97 (1992).

[36] R. A. Bank, M. T. Bayliss, F. P. Lafeber, A. Maroudas, and J. M. Tekoppele, "Ageing and zonal variation in post-translational modification of collagen in normal human articular cartilage. The age-related increase in non-enzymatic glycation affects biomechanical properties of cartilage.," *The Biochemical journal* **330 (Pt 1,** 345–51 (1998).

[37] D. Eyre, "Collagen of articular cartilage.," *Arthritis research* **4,** 30–5 (2002).

[38] G. E. Kempson, M. A. Freeman, and S. A. Swanson, "Tensile properties of articular cartilage.," *Nature* **220,** 1127–8 (1968).

[39] V. C. Mow and M. Lai, "Biorheology of swelling tissue.," *Biorheology* **27,** 110–9 (1990).

[40] M. Venn and A. Maroudas, "Chemical composition and swelling of normal and osteoarthrotic femoral head cartilage. I. Chemical composition.," *Annals of the rheumatic diseases* **36,** 121–9 (1977).

[41] J. P. Arokoski, M. M. Hyttinen, T. Lapveteläinen, P. Takács, B. Kosztáczky, L. Módis, V. Kovanen, and H. Helminen, "Decreased birefringence of the superficial zone collagen network in the canine knee (stifle) articular cartilage after long distance running training, detected by quantitative polarised light microscopy.," *Annals of the rheumatic diseases* **55,** 253–64 (1996).

[42] U. Duvvuri, S. R. Charagundla, S. B. Kudchodkar, J. H. Kaufman, J. B. Kneeland, R. Rizi, J. S. Leigh, and R. Reddy, "Human knee: in vivo T1(rho)-weighted MR imaging at 1.5 T–preliminary experience.," *Radiology* **220,** 822–6 (2001).

[43] E. M. Shapiro, A. Borthakur, J. H. Kaufman, J. S. Leigh, and R. Reddy, "Water distribution patterns inside bovine articular cartilage as visualized by 1H magnetic resonance imaging.," *Osteoarthritis and cartilage* **9,** 533–8 (2001).

[44] J. S. Jurvelin, D. J. Müller, M. Wong, D. Studer, A. Engel, and E. B. Hunziker, "Surface and subsurface morphology of bovine humeral articular cartilage as assessed by atomic force and transmission electron microscopy.," *Journal of structural biology* **117,** 45–54 (1996).

[45] J. M. Clark, "The organisation of collagen fibrils in the superficial zones of articular cartilage.," *Journal of anatomy* **171,** 117–30 (1990).

[46] I. Redler, "A scanning electron microscopic study of human normal and osteoarthritic articular cartilage.," *Clinical orthopaedics and related research* 262–8 (1974).

[47] E. Fragonas, V. Mlynárik, V. Jellús, F. Micali, A. Piras, R. Toffanin, R. Rizzo, and F. Vittur, "Correlation between biochemical composition and magnetic resonance appearance of articular cartilage.," *Osteoarthritis and cartilage* **6,** 24–32 (1998).

[48] S. Gomez, R. Toffanin, S. Bernstorff, M. Romanello, H. Amenitsch, M. Rappolt, R. Rizzo, and F. Vittur, "Collagen fibrils are differently organized in weight-bearing and not-weight-bearing regions of pig articular cartilage.," *The Journal of experimental zoology* **287,** 346–52 (2000).

[49] Y. Xia, J. B. Moody, and H. Alhadlaq, "Orientational dependence of T2 relaxation in articular cartilage: A microscopic MRI (microMRI) study.," *Magnetic resonance in medicine : official journal of the Society of Magnetic Resonance in Medicine / Society of Magnetic Resonance in Medicine* **48,** 460–9 (2002).

[50] J. Rieppo, E. P. Halmesmäki, U. Siitonen, M. S. Laasanen, J. Töyras, I. Kiviranta, M. M. Hyttinen, J. S. Jurvelin, and H. J. Helminen, "Histological differences of human, bovine and porcine cartilage.," *Trans Orthop Res Soc* **28** (2003).

[51] V. C. Mow, A. Ratcliffe, M. P. Rosenwasser, and J. A. Buckwalter, "Experimental studies on repair of large osteochondral defects at a high weight bearing area of the knee joint: a tissue engineering study.," *Journal of biomechanical engineering* **113,** 198–207 (1991).

[52] H. Muir, "Proteoglycans as organizers of the intercellular matrix.," *Biochemical Society transactions* **11,** 613–22 (1983).

[53] H. Muir, P. Bullough, and A. Maroudas, "The distribution of collagen in human articular cartilage with some of its physiological implications.," *The Journal of bone and joint surgery. British volume* **52,** 554–63 (1970).

[54] M. Huber, S. Trattnig, and F. Lintner, "Anatomy, biochemistry, and physiology of articular cartilage.," *Investigative radiology* **35,** 573–80 (2000).

[55] E. B. Hunziker, "Articular cartilage repair: basic science and clinical progress. A review of the current status and prospects.," *Osteoarthritis and cartilage* **10,** 432–63 (2002).

[56] R. A. Stockwell, "Chondrocytes.," *Journal of clinical pathology. Supplement (Royal College of Pathologists)* **12,** 7–13 (1978).

[57] D. H. Collins and T. F. McElligott, "Sulphate (35SO4) uptake by chondrocytes in relation to histological changes in osteoarthritic human articular cartilage.," *Annals of the rheumatic diseases* **19,** 318–30 (1960).

[58] H. Muir, "The chondrocyte, architect of cartilage. Biomechanics, structure, function and molecular biology of cartilage matrix macromolecules.," *BioEssays : news and reviews in molecular, cellular and developmental biology* **17,** 1039–48 (1995).

[59] A. Maroudas and R. Schneiderman, ""Free" and "exchangeable" or "trapped" and "non-exchangeable" water in cartilage.," *Journal of orthopaedic research : official publication of the Orthopaedic Research Society* **5,** 133–8 (1987).

[60] G. D. Jay, J. R. Torres, M. L. Warman, M. C. Laderer, and K. S. Breuer, "The role of lubricin in the mechanical behavior of synovial fluid.," *Proceedings of the National Academy of Sciences of the United States of America* **104,** 6194–9 (2007).

[61] R. K. Lemperg, S. E. Larsson, and S. O. Hjertquist, "Distribution of water and glycosaminoglycans in different layers of cattle articular cartilage.," *Israel journal of medical sciences* **7,** 419–21 (1971).

[62] R. Brocklehurst, M. T. Bayliss, A. Maroudas, H. L. Coysh, M. A. Freeman, P. A. Revell, and S. Y. Ali, "The composition of normal and osteoarthritic articular cartilage from human knee joints. With special reference to unicompartmental replacement and osteotomy of the knee.," *The Journal of bone and joint surgery. American volume* **66,** 95–106 (1984).

[63] A. I. Maroudas, "Balance between swelling pressure and collagen tension in normal and degenerate cartilage.," *Nature* **260,** 808–9 (1976).

[64] W. Wilson, C. C. van Donkelaar, B. van Rietbergen, and R. Huiskes, "A fibril-reinforced poroviscoelastic swelling model for articular cartilage.," *Journal of biomechanics* **38,** 1195–204 (2005).

[65] V. C. Mow, S. C. Kuei, W. M. Lai, and C. G. Armstrong, "Biphasic creep and stress relaxation of articular cartilage in compression? Theory and experiments.," *Journal of biomechanical engineering* **102,** 73–84 (1980).

[66] W. C. Hayes and A. J. Bodine, "Flow-independent viscoelastic properties of articular cartilage matrix.," *Journal of biomechanics* **11,** 407–19 (1978).

[67] C.-L. Lee, M.-H. Huang, C.-Y. Chai, C.-H. Chen, J.-Y. Su, and Y.-C. Tien, "The validity of in vivo ultrasonographic grading of osteoarthritic femoral condylar cartilage: a comparison with in vitro ultrasonographic and histologic gradings.," *Osteoarthritis and cartilage* **16,** 352–8 (2008).

[68] H. J. Mankin and L. Lippiello, "Biochemical and metabolic abnormalities in articular cartilage from osteo-arthritic human hips.," *The Journal of bone and joint surgery. American volume* **52,** 424–34 (1970).

[69] H. J. Nieminen, Y. Zheng, S. Saarakkala, Q. Wang, J. Töyräs, Y. Huang, and J. S. Jurvelin, "Quantitative assessment of articular cartilage using high-frequency ultrasound: research findings and diagnostic prospects.," *Critical reviews in biomedical engineering* **37,** 461–94 (2009).

[70] R. M. Aspden and D. W. Hukins, "Collagen organization in articular cartilage, determined by X-ray diffraction, and its relationship to tissue function.," *Proceedings of the Royal Society*

of London. Series B, Containing papers of a Biological character. Royal Society (Great Britain) **212,** 299–304 (1981).

[71] M. T. Nieminen, J. Töyräs, J. Rieppo, J. M. Hakumäki, J. Silvennoinen, H. J. Helminen, and J. S. Jurvelin, "Quantitative MR microscopy of enzymatically degraded articular cartilage.," *Magnetic resonance in medicine : official journal of the Society of Magnetic Resonance in Medicine / Society of Magnetic Resonance in Medicine* **43,** 676–81 (2000).

[72] H. J. Nieminen, P. Julkunen, J. Töyräs, and J. S. Jurvelin, "Ultrasound speed in articular cartilage under mechanical compression.," *Ultrasound in medicine & biology* **33,** 1755–66 (2007).

[73] X. L. Lu and V. C. Mow, "Biomechanics of articular cartilage and determination of material properties.," *Medicine and science in sports and exercise* **40,** 193–9 (2008).

[74] M. A. Soltz and G. A. Ateshian, "Experimental verification and theoretical prediction of cartilage interstitial fluid pressurization at an impermeable contact interface in confined compression.," *Journal of biomechanics* **31,** 927–34 (1998).

[75] H. T. Kokkonen, J.-S. Suomalainen, A. Joukainen, H. Kröger, J. Sirola, J. S. Jurvelin, J. Salo, and J. Töyräs, "In vivo diagnostics of human knee cartilage lesions using delayed CBCT arthrography.," *Journal of orthopaedic research : official publication of the Orthopaedic Research Society* 1–10 (2013).

[76] A. Maroudas, H. Muir, and J. Wingham, "The correlation of fixed negative charge with glycosaminoglycan content of human articular cartilage.," *Biochimica et biophysica acta* **177,** 492–500 (1969).

[77] T. J. Perlewitz, V. M. Haughton, L. H. Riley, C. Nguyen-Minh, and V. George, "Effect of molecular weight on the diffusion of contrast media into cartilage.," *Spine* **22,** 2707–10 (1997).

[78] G. A. Ateshian, "The role of interstitial fluid pressurization in articular cartilage lubrication.," *Journal of biomechanics* **42,** 1163–76 (2009).

[79] J. A. Buckwalter, J. A. Martin, and T. D. Brown, "Perspectives on chondrocyte mechanobiology and osteoarthritis.," *Biorheology* **43,** 603–9 (2006).

[80] P. Dieppe, "Disease modification in osteoarthritis: are drugs the answer?," *Arthritis and rheumatism* **52,** 1956–9 (2005).

[81] J. A. Buckwalter and H. J. Mankin, "Articular cartilage: degeneration and osteoarthritis, repair, regeneration, and transplantation.," *Instructional course lectures* **47,** 487–504 (1998).

[82] J. Haapala, J. P. Arokoski, M. M. Hyttinen, M. Lammi, M. Tammi, V. Kovanen, H. J. Helminen, and I. Kiviranta, "Remobilization does not fully restore immobilization induced articular cartilage atrophy.," *Clinical orthopaedics and related research* 218–29 (1999).

[83] M. J. Palmoski and K. D. Brandt, "Running inhibits the reversal of atrophic changes in canine knee cartilage after removal of a leg cast.," *Arthritis and rheumatism* **24,** 1329–37 (1981).

[84] L. A. Setton, V. C. Mow, F. J. Müller, J. C. Pita, and D. S. Howell, "Mechanical behavior and biochemical composition of canine knee cartilage following periods of joint disuse and disuse with remobilization.," *Osteoarthritis and cartilage* **5,** 1–16 (1997).

[85] A. M. Säämänen, M. Tammi, J. Jurvelin, I. Kiviranta, and H. J. Helminen, "Proteoglycan alterations following immobilization and remobilization in the articular cartilage of young canine knee (stifle) joint.," *Journal of orthopaedic research : official publication of the Orthopaedic Research Society* **8,** 863–73 (1990).

[86] D. M. Freeman, G. Bergman, and G. Glover, "Short TE MR microscopy: accurate measurement and zonal differentiation

of normal hyaline cartilage.," *Magnetic resonance in medicine : official journal of the Society of Magnetic Resonance in Medicine / Society of Magnetic Resonance in Medicine* **38,** 72–81 (1997).

[87] H. Sandmark and E. Vingå rd, "Sports and risk for severe osteoarthrosis of the knee.," *Scandinavian journal of medicine & science in sports* **9,** 279–84 (1999).

[88] R. Altman, E. Asch, D. Bloch, G. Bole, D. Borenstein, K. Brandt, W. Christy, T. D. Cooke, R. Greenwald, and M. Hochberg, "Development of criteria for the classification and reporting of osteoarthritis. Classification of osteoarthritis of the knee. Diagnostic and Therapeutic Criteria Committee of the American Rheumatism Association.," *Arthritis and rheumatism* **29,** 1039–49 (1986).

[89] R. C. Lawrence, D. T. Felson, C. G. Helmick, L. M. Arnold, H. Choi, R. A. Deyo, S. Gabriel, R. Hirsch, M. C. Hochberg, G. G. Hunder, J. M. Jordan, J. N. Katz, H. M. Kremers, and F. Wolfe, "Estimates of the prevalence of arthritis and other rheumatic conditions in the United States. Part II.," *Arthritis and rheumatism* **58,** 26–35 (2008).

[90] J. H. KELLGREN and J. S. LAWRENCE, "Radiological assessment of osteo-arthrosis.," *Annals of the rheumatic diseases* **16,** 494–502 (1957).

[91] F. Eckstein, H. Sittek, S. Milz, R. Putz, and M. Reiser, "The morphology of articular cartilage assessed by magnetic resonance imaging (MRI). Reproducibility and anatomical correlation.," *Surgical and radiologic anatomy : SRA* **16,** 429–38 (1994).

[92] M. J. Nissi, F. Toth, J. Zhang, S. Schmitter, M. Benson, C. S. Carlson, and J. M. Ellermann, "Susceptibility weighted imaging of cartilage canals in porcine epiphyseal growth cartilage ex vivo and in vivo.," *Magnetic resonance in medicine : official*

journal of the Society of Magnetic Resonance in Medicine / Society of Magnetic Resonance in Medicine **71,** 2197–205 (2014).

[93] J. Honkanen, E. Danso, J.-S. Suomalainen, V. Tiitu, R. Korhonen, J. Jurvelin, and J. Töyräs, "Diffusion Contrast Enhanced Imaging of Human Meniscus Using Cone Beam CT.," *Osteoarthritis and cartilage* (2014).

[94] M. Brittberg and C. S. Winalski, "Evaluation of cartilage injuries and repair.," *The Journal of bone and joint surgery. American volume* **85-A Suppl,** 58–69 (2003).

[95] G. Spahn, H. M. Klinger, T. Mückley, and G. O. Hofmann, "Four-year results from a randomized controlled study of knee chondroplasty with concomitant medial meniscectomy: mechanical debridement versus radiofrequency chondroplasty.," *Arthroscopy : the journal of arthroscopic & related surgery : official publication of the Arthroscopy Association of North America and the International Arthroscopy Association* **26,** S73–80 (2010).

[96] N. Gerwin, C. Hops, and A. Lucke, "Intraarticular drug delivery in osteoarthritis.," *Advanced drug delivery reviews* **58,** 226–42 (2006).

[97] A. Bedi, B. T. Feeley, and R. J. Williams, "Management of articular cartilage defects of the knee.," *The Journal of bone and joint surgery. American volume* **92,** 994–1009 (2010).

[98] M. Brittberg, "Autologous chondrocyte implantation–technique and long-term follow-up.," *Injury* **39 Suppl 1,** S40–9 (2008).

[99] P. D. Gikas, W. J. S. Aston, and T. W. R. Briggs, "Autologous chondrocyte implantation: where do we stand now?," *Journal of orthopaedic science : official journal of the Japanese Orthopaedic Association* **13,** 283–92 (2008).

[100] I. Bjarnason, J. Hayllar, A. J. MacPherson, and A. S. Russell, "Side effects of nonsteroidal anti-inflammatory drugs on the small and large intestine in humans.," *Gastroenterology* **104,** 1832–47 (1993).

[101] I. Bjarnason, "Gastrointestinal safety of NSAIDs and over-the-counter analgesics.," *International journal of clinical practice. Supplement* 37–42 (2013).

[102] X. Yang, H. Du, and G. Zhai, "Progress in intra-articular drug delivery systems for osteoarthritis.," *Current drug targets* **15,** 888–900 (2014).

[103] H. J. Nieminen, a. Salmi, P. Karppinen, E. Hæ ggström, and S. a. Hacking, "The potential utility of high-intensity ultrasound to treat osteoarthritis.," *Osteoarthritis and cartilage* **22,** 1784–1799 (2014).

[104] H. A. Breinan, S. D. Martin, H. P. Hsu, and M. Spector, "Healing of canine articular cartilage defects treated with microfracture, a type-II collagen matrix, or cultured autologous chondrocytes.," *Journal of orthopaedic research : official publication of the Orthopaedic Research Society* **18,** 781–9 (2000).

[105] K. Mithoefer, R. J. Williams, R. F. Warren, H. G. Potter, C. R. Spock, E. C. Jones, T. L. Wickiewicz, and R. G. Marx, "Chondral resurfacing of articular cartilage defects in the knee with the microfracture technique. Surgical technique.," *The Journal of bone and joint surgery. American volume* **88 Suppl 1,** 294–304 (2006).

[106] L. Hangody and P. Füles, "Autologous osteochondral mosaicplasty for the treatment of full-thickness defects of weight-bearing joints: ten years of experimental and clinical experience.," *The Journal of bone and joint surgery. American volume* **85-A Suppl,** 25–32 (2003).

[107] L. Hangody, G. Kish, Z. Kárpáti, I. Szerb, and I. Udvarhelyi, "Arthroscopic autogenous osteochondral mosaicplasty

for the treatment of femoral condylar articular defects. A preliminary report.," *Knee surgery, sports traumatology, arthroscopy : official journal of the ESSKA* **5,** 262–7 (1997).

[108] M. Brittberg, E. Faxén, and L. Peterson, "Carbon fiber scaffolds in the treatment of early knee osteoarthritis. A prospective 4-year followup of 37 patients.," *Clinical orthopaedics and related research* 155–64 (1994).

[109] J. N. Katz, "Total joint replacement in osteoarthritis.," *Best practice & research. Clinical rheumatology* **20,** 145–53 (2006).

[110] M. B. Goldring and S. R. Goldring, "Articular cartilage and subchondral bone in the pathogenesis of osteoarthritis.," *Annals of the New York Academy of Sciences* **1192,** 230–7 (2010).

[111] E. L. Radin and R. M. Rose, "Role of subchondral bone in the initiation and progression of cartilage damage.," *Clinical orthopaedics and related research* 34–40 (1986).

[112] D. T. Felson, "Weight and osteoarthritis.," *The American journal of clinical nutrition* **63,** 430S–432S (1996).

[113] P. N. Wells, *Physical Principles of Ultrasonic Diagnosis.* (Academic Pres., New York, 1969).

[114] E. L. Madsen, H. J. Sathoff, and J. A. Zagzebski, "Ultrasonic shear wave properties of soft tissues and tissuelike materials.," *The Journal of the Acoustical Society of America* **74,** 1346–55 (1983).

[115] L. A. Frizzell and E. L. Carstensen, "Shear properties of mammalian tissues at low megahertz frequencies.," *The Journal of the Acoustical Society of America* **60,** 1409–11 (1976).

[116] P. J. Shull, *Nondestructive Evaluation: Theory, Techniques, and Applications* (CRC Press, 2002).

[117] L. E. Kinsler, *Fundamentals of acoustics* (Wiley, New York, 2000).

[118] F. Duck, A. Baker, and H. Starritt, *Ultrasound in medicine* (IOP publishing Ltd, Bristol, 1998).

[119] P. N. Wells, "Review: absorption and dispersion of ultrasound in biological tissue.," *Ultrasound in medicine & biology* **1,** 369–76 (1975).

[120] B. A. Auld, *Acoustic Fields and Waves in Solids, Vols. 1-2* (Krieger Publishing Company, 1990).

[121] L. Ferrari and J. P. Jones, "The propagation of Gaussian modulated pulses in dissipative and/or dispersive media such as tissue.," *Ultrasound in medicine & biology* **11,** 299–305 (1985).

[122] J. Joule, "On the effects of magnetism on the dimensions of iron and steel bars.," *Phil Mag* **30,** 226–241 (1847).

[123] B. Langenecker, "Interaction of Ultrasound with Magnetic Domains and Dislocations.," *Journal of Applied Physics* **37,** 999 (1966).

[124] A. P. Edson and E. L. Huston, "High performance magnetostrictive transducers.," (1974).

[125] D. Legros, J. Lewiner, and P. Biquard, "Generation of ultrasound by dielectric transducer.," *Journal of the Acoustical Society of America* **52,** 196–198 (1972).

[126] D. Legros and J. Lewiner, "Electrostatic ultrasonic transducers and their utilization with foil electrets.," *Journal of the Acoustical Society of America* **53,** 1663–1672 (1973).

[127] O. Oralkan, A. S. Ergun, J. A. Johnson, M. Karaman, U. Demirci, K. Kaviani, T. H. Lee, and B. T. Khuri-Yakub, "Capacitive micromachined ultrasonic transducers: next-generation arrays for acoustic imaging?," *IEEE transactions on ultrasonics, ferroelectrics, and frequency control* **49,** 1596–610 (2002).

[128] A. Manbachi and R. S. C. Cobbold, "Development and application of piezoelectric materials for ultrasound generation and detection.," *Ultrasound* **19,** 187–196 (2011).

[129] G. A. Joiner, E. R. Bogoch, K. P. Pritzker, M. D. Buschmann, A. Chevrier, and F. S. Foster, "High frequency acoustic parameters of human and bovine articular cartilage following experimentally-induced matrix degradation.," *Ultrasonic imaging* **23,** 106–16 (2001).

[130] H. Y. Ling, Y. P. Zheng, and S. G. Patil, "Strain dependence of ultrasound speed in bovine articular cartilage under compression in vitro.," *Ultrasound in medicine & biology* **33,** 1599–608 (2007).

[131] H. J. Nieminen, S. Saarakkala, M. S. Laasanen, J. Hirvonen, J. S. Jurvelin, and J. Töyräs, "Ultrasound attenuation in normal and spontaneously degenerated articular cartilage.," *Ultrasound in medicine & biology* **30,** 493–500 (2004).

[132] B. Jaffré, A. Watrin, D. Loeuille, P. Gillet, P. Netter, P. Laugier, and A. Saïed, "Effects of antiinflammatory drugs on arthritic cartilage: a high-frequency quantitative ultrasound study in rats.," *Arthritis and rheumatism* **48,** 1594–601 (2003).

[133] M. S. Laasanen, S. Saarakkala, J. Töyräs, J. Rieppo, and J. S. Jurvelin, "Site-specific ultrasound reflection properties and superficial collagen content of bovine knee articular cartilage.," *Physics in medicine and biology* **50,** 3221–33 (2005).

[134] B. Pellaumail, D. Loeuille, A. Watrin, P. Netter, G. Berger, and A. Saied, "Correlation of high frequency ultrasound backscatter with cartilage matrix constituents.," in *1998 IEEE Ultrasonics Symposium. Proceedings (Cat. No. 98CH36102)*, Vol. 2 (1998), pp. 1463–1466.

[135] J. Töyräs, M. S. Laasanen, S. Saarakkala, M. J. Lammi, J. Rieppo, J. Kurkijärvi, R. Lappalainen, and J. S. Jurvelin,

"Speed of sound in normal and degenerated bovine articular cartilage.," *Ultrasound in Medicine & Biology* **29,** 447–454 (2003).

[136] I. Youn, F. H. Fu, and J.-K. Suh, "Determination of the mechanical properties of articular cartilage using a high-frequency ultrasonic indentation technique.," *Trans Orthop Res Soc* **23,** 162 (1999).

[137] S. Lees, J. D. Heeley, J. M. Ahern, and M. G. Oravecz, "Axial phase velocity in rat tail tendon fibers at 100 MHz by ultrasonic microscopy.," *IEEE Trans Sonics Ultrason* **30(2),** 85–90 (1983).

[138] S. G. Patil, Y. P. Zheng, J. Y. Wu, and J. Shi, "Measurement of depth-dependence and anisotropy of ultrasound speed of bovine articular cartilage in vitro.," *Ultrasound in medicine & biology* **30,** 953–63 (2004).

[139] E. Chérin, A. Säıed, and P. Laugier, "Evaluation of acoustical parameter sensitivity to age-related and osteoarthritic changes in articular cartilage using 50-MHz ultrasound.," *Ultrasound in medicine & biology* **24,** 341–354 (1998).

[140] D. H. Agemura, W. D. O'Brien, J. E. Olerud, L. E. Chun, and D. E. Eyre, "Ultrasonic propagation properties of articular cartilage at 100 MHz.," *The Journal of the Acoustical Society of America* **87,** 1786–91 (1990).

[141] D. A. Senzig, F. K. Forster, and J. E. Olerud, "Ultrasonic attenuation in articular cartilage.," *The Journal of the Acoustical Society of America* **92,** 676–81 (1992).

[142] S. Saarakkala, R. K. Korhonen, M. S. Laasanen, J. Töyräs, J. Rieppo, and J. S. Jurvelin, "Mechano-acoustic determination of Young's modulus of articular cartilage.," *Biorheology* **41,** 167–79 (2004).

[143] E. Chaljub, D. Komatitsch, J. P. Vilotte, Y. Capdeville, B. Valette, and G. Festa, *Advances in Wave Propagation in Heterogenous Earth*, Vol. 48 of *Advances in Geophysics* (Elsevier, 2007).

[144] H. Takenaka, T. Furumura, and H. Fujiwara, "Recent developments in numerical methods for ground motion simulation.," in *Proc. 2-nd International Symposium on the Effects of Surface Geology on Seismic Motion* (1998), pp. 91–101.

[145] R. G. Pratt and M. H. Worthington, "Inverse theory applied to multi-source cross-hole tomography. Part 1. Acoustic wave-equation method.," *Geophysical Prospecting* **38,** 287–310 (1990).

[146] R. G. Pratt, C. Shin, and G. J. Hicks, "Gauss-Newton and full Newton methods in frequency-space seismic waveform inversion.," *Geophysical Journal International* **133,** 341–362 (1998).

[147] V. Thomée, "From finite differences to finite elements.," *Journal of Computational and Applied Mathematics* **128,** 1–54 (2001).

[148] G. E. Forsythe and W. R. Wasow, *Finite-Difference Methods for Partial Differential Equations* (J. Wiley & Sons, New York, 1960).

[149] K. S. Yee, "Numerical Solution.," *IEEE Transactions on antennas and propagation* **14,** 302–307 (1966).

[150] E. Isaacson and H. B. Keller, *Analysis of Numerical Methods* (J. Wiley & Sons, New York, 1966).

[151] R. D. Richtmyer and K. W. Morton, *Difference Methods for Initial Value Problems* (J. Wiley & Sons, New York, 1967).

[152] A. Taflove, "Application of the Finite-Difference Time-Domain Method to Sinusoidal Steady-State Electromagnetic-Penetration Problems.," *IEEE Transactions on electromagnetic compatibility* **22,** 191–202 (1980).

[153] J. C. Maxwell, "A dynamical theory of the electromagnetic field," *Philosophical Transactions of the Royal Society of London* **155,** 459–512 (1865).

[154] K. F. Graff, *Wave motion in elastic solids* (The Clarendon Press, Oxford, 1975).

[155] J. J. Kaufman, G. Luo, and R. S. Siffert, "Ultrasound simulation for 3D-axisymmetric models.," in *2003 IEEE Symposium on ultrasonics*, Vol. 00 (2003), pp. 2065–2068.

[156] P. P. Delsanto, R. S. Schechterb, and R. B. Mignogna, "Connection machine simulation of ultrasonic wave propagation in materials III : The three-dimensional case.," *Wave motion* **26,** 329–339 (1997).

[157] J. E. Kurkijärvi, M. J. Nissi, I. Kiviranta, J. S. Jurvelin, and M. T. Nieminen, "Delayed gadolinium-enhanced MRI of cartilage (dGEMRIC) and T2 characteristics of human knee articular cartilage: topographical variation and relationships to mechanical properties.," *Magnetic resonance in medicine : official journal of the Society of Magnetic Resonance in Medicine / Society of Magnetic Resonance in Medicine* **52,** 41–6 (2004).

[158] C.-J. Qu, J. Rieppo, M. M. Hyttinen, M. J. Lammi, I. Kiviranta, J. Kurkijärvi, J. S. Jurvelin, and J. Töyräs, "Human articular cartilage proteoglycans are not undersulfated in osteoarthritis.," *Connective tissue research* **48,** 27–33 (2007).

[159] T. S. Silvast, J. S. Jurvelin, M. J. Lammi, and J. Töyräs, "pQCT study on diffusion and equilibrium distribution of iodinated anionic contrast agent in human articular cartilage–associations to matrix composition and integrity.," *Osteoarthritis and cartilage* **17,** 26–32 (2009).

[160] P. Kiviranta, E. Lammentausta, J. Töyräs, I. Kiviranta, and J. S. Jurvelin, "Indentation diagnostics of cartilage degeneration.," *Osteoarthritis and cartilage* **16,** 796–804 (2008).

[161] M. S. Laasanen, J. Töyräs, J. Hirvonen, S. Saarakkala, R. K. Korhonen, M. T. Nieminen, I. Kiviranta, and J. S. Jurvelin, "Novel mechano-acoustic technique and instrument for diagnosis of cartilage degeneration.," *Physiological measurement* **23,** 491–503 (2002).

[162] R. K. Korhonen, M. S. Laasanen, J. Töyräs, J. Rieppo, J. Hirvonen, H. J. Helminen, and J. S. Jurvelin, "Comparison of the equilibrium response of articular cartilage in unconfined compression, confined compression and indentation.," *Journal of biomechanics* **35,** 903–9 (2002).

[163] W. C. Hayes, L. M. Keer, G. Herrmann, and L. F. Mockros, "A mathematical analysis for indentation tests of articular cartilage.," *Journal of biomechanics* **5,** 541–51 (1972).

[164] N. P. Camacho, P. West, P. a. Torzilli, and R. Mendelsohn, "FTIR microscopic imaging of collagen and proteoglycan in bovine cartilage.," *Biopolymers* **62,** 1–8 (2001).

[165] L. Rieppo, S. Saarakkala, T. Närhi, J. Holopainen, M. Lammi, H. J. Helminen, J. S. Jurvelin, and J. Rieppo, "Quantitative analysis of spatial proteoglycan content in articular cartilage with Fourier transform infrared imaging spectroscopy: Critical evaluation of analysis methods and specificity of the parameters.," *Microscopy research and technique* **73,** 503–12 (2010).

[166] L. Rieppo, S. Saarakkala, J. S. Jurvelin, and J. Rieppo, "Prediction of compressive stiffness of articular cartilage using Fourier transform infrared spectroscopy.," *Journal of biomechanics* **46,** 1269–75 (2013).

[167] A. Fedorov, R. Beichel, J. Kalpathy-Cramer, J. Finet, J.-C. Fillion-Robin, S. Pujol, C. Bauer, D. Jennings, F. Fennessy, M. Sonka, J. Buatti, S. Aylward, J. V. Miller, S. Pieper, and R. Kikinis, "3D Slicer as an image computing platform for the Quantitative Imaging Network.," *Magnetic resonance imaging* **30,** 1323–41 (2012).

[168] I. H. Muir, "Biochemistry of articular cartilage in rheumatic diseases.," *Scandinavian journal of rheumatology. Supplement* **38,** 25–9 (1980).

[169] H. Fischer, I. Polikarpov, and A. F. Craievich, "Average protein density is a molecular-weight-dependent function.," *Protein science : a publication of the Protein Society* **13,** 2825–8 (2004).

[170] S. Saarakkala, M. S. Laasanen, J. S. Jurvelin, K. Törrönen, M. J. Lammi, R. Lappalainen, and J. Töyräs, "Ultrasound indentation of normal and spontaneously degenerated bovine articular cartilage.," *Osteoarthritis and cartilage* **11,** 697–705 (2003).

[171] M. B. Goldring, "Articular cartilage degradation in osteoarthritis.," *HSS journal : the musculoskeletal journal of Hospital for Special Surgery* **8,** 7–9 (2012).

[172] M. A. Hakulinen, J. S. Day, J. Töyräs, H. Weinans, and J. S. Jurvelin, "Ultrasonic characterization of human trabecular bone microstructure.," *Physics in medicine and biology* **51,** 1633–48 (2006).

[173] J. Karjalainen, O. Riekkinen, J. Töyräs, H. Kröger, and J. Jurvelin, "Ultrasonic assessment of cortical bone thickness *in vitro* and *in vivo*.," *IEEE transactions on ultrasonics, ferroelectrics, and frequency control* **55,** 2191–7 (2008).

[174] J. P. Karjalainen, O. Riekkinen, J. Töyräs, M. Hakulinen, H. Kröger, T. Rikkonen, K. Salovaara, and J. S. Jurvelin, "Multi-site bone ultrasound measurements in elderly women with and without previous hip fractures.," *Osteoporosis international : a journal established as result of cooperation between the European Foundation for Osteoporosis and the National Osteoporosis Foundation of the USA* **23,** 1287–95 (2012).

[175] B. K. Hoffmeister, D. P. Johnson, J. A. Janeski, D. A. Keedy, B. W. Steinert, A. M. Viano, and S. C. Kaste, "Ultrasonic characterization of human cancellous bone in vitro using three

different apparent backscatter parameters in the frequency range 0.6-15.0 MHz.," *IEEE transactions on ultrasonics, ferroelectrics, and frequency control* **55,** 1442–52 (2008).

[176] B. K. Hoffmeister, A. P. Holt, and S. C. Kaste, "Effect of the cortex on ultrasonic backscatter measurements of cancellous bone.," *Physics in medicine and biology* **56,** 6243–55 (2011).

[177] W. R. Jones, H. P. Ting-Beall, G. M. Lee, S. S. Kelley, R. M. Hochmuth, and F. Guilak, "Alterations in the Young's modulus and volumetric properties of chondrocytes isolated from normal and osteoarthritic human cartilage.," *Journal of biomechanics* **32,** 119–27 (1999).

[178] F. Eckstein, M. Matsuura, V. Kuhn, M. Priemel, R. Müller, T. M. Link, and E.-M. Lochmüller, "Sex differences of human trabecular bone microstructure in aging are site-dependent.," *Journal of bone and mineral research : the official journal of the American Society for Bone and Mineral Research* **22,** 817–24 (2007).

[179] E. Kaleva, S. Saarakkala, J. S. Jurvelin, T. Virén, and J. Töyräs, "Effects of ultrasound beam angle and surface roughness on the quantitative ultrasound parameters of articular cartilage.," *Ultrasound in medicine & biology* **35,** 1344–51 (2009).

[180] J. K. Suh, I. Youn, and F. H. Fu, "An *in situ* calibration of an ultrasound transducer: a potential application for an ultrasonic indentation test of articular cartilage.," *Journal of biomechanics* **34,** 1347–53 (2001).

Jukka Liukkonen

Ultrasound Arthroscopy of Articular Cartilage and Subchondral Bone

Millions of arthroscopies are annually performed worldwide. Arthroscopic diagnosis should be immediate, sensitive and reproducible. However, conventional arthroscopic evaluation of cartilage is subjective and poorly reproducible. In this thesis, the feasibility of ultrasound arthroscopy for diagnostics of joint disorders was in investigated *in vitro* and *in vivo,* and ultrasound interactions in cartilage tissue were modeled using finite difference time domain method. Ultrasound arthroscopy was found to provide valuable information on cartilage. The numerical models introduced in this thesis may provide significant help for interpretation of the results of ultrasound assessment of cartilage and subchondral bone.

UNIVERSITY OF
EASTERN FINLAND

Publications of the University of Eastern Finland
Dissertations in Forestry and Natural Sciences

ISBN 978-952-61-1756-0